Cell Reports

Article

Lateralization of short-term memory in the frontal cortex

Graphical abstract

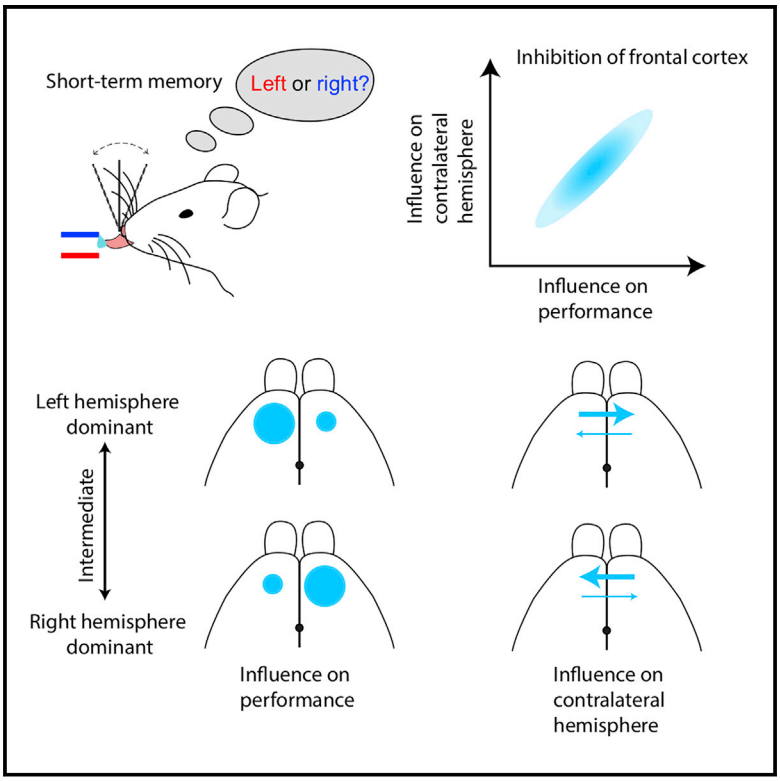

Authors

Xinxin Yin, Yu Wang, Jiejue Li, Zengcai V. Guo

Correspondence

guozengcai@tsinghua.edu.cn

In brief

The left and right brain do not contribute equally to cognition. Yin et al. find that the frontal cortex shows left- or right-brain dominance during short-term memory in a sensory-motor association dependent way. The dominant hemisphere influences coding activity in the non-dominant hemisphere, but not vice versa.

Highlights

- The frontal cortex shows left- or right-brain dominance in short-term memory
- The left and right frontal cortex have similar neural dynamics
- The dominant hemisphere regulates neural activity in the non-dominant hemisphere
- Asymmetric hemispheric interaction determines dominance and behavioral variability

Yin et al., 2022, Cell Reports *40*, 111190
August 16, 2022
https://doi.org/10.1016/j.celrep.2022.111190

CellPress

Cell Reports

CellPress
OPEN ACCESS

Article

Lateralization of short-term memory in the frontal cortex

Xinxin Yin,[1,2,3,4] Yu Wang,[2,3,4] Jiejue Li,[2,3,4] and Zengcai V. Guo[1,2,3,5,*]
[1]School of Medicine, Tsinghua University, 100084 Beijing, China
[2]IDG/McGovern Institute for Brain Research, Tsinghua University, 100084 Beijing, China
[3]Tsinghua-Peking Joint Center for Life Sciences, 100084 Beijing, China
[4]School of Life Sciences, Tsinghua University, 100084 Beijing, China
[5]Lead contact
*Correspondence: guozengcai@tsinghua.edu.cn
https://doi.org/10.1016/j.celrep.2022.111190

SUMMARY

Despite essentially symmetric structures in mammalian brains, the left and right hemispheres do not contribute equally to certain cognitive functions. How both hemispheres interact to cause this asymmetry remains unclear. Here, we study this question in the anterior lateral motor cortex (ALM) of mice performing five versions of a tactile-based decision-making task with a short-term memory (STM) component. Unilateral inhibition of ALM produces variable behavioral deficits across tasks, with the left, right, or both ALMs playing critical roles in STM. Neural activity and its encoding capability are similar across hemispheres, despite that only one hemisphere dominates in behavior. Inhibition of the dominant ALM disrupts encoding capability in the non-dominant ALM, but not vice versa. Variable behavioral deficits are predicted by the influence on contralateral activity across sessions, mice, and tasks. Together, these results reveal that the left and right ALM interact asymmetrically, leading to their differential contributions to STM.

INTRODUCTION

The macrostructure of the two hemispheres in mammalian brains appears to be nearly identical (Defelipe, 2011). However, various brain functions are preferentially localized to one hemisphere. For example, classical lesion studies identified the Broca's and Wernicke's areas (the two centers for speech processing) typically in the left hemisphere (Bogen and Bogen, 1976; Dronkers et al., 2007). Research on split-brain patients suggests that each hemisphere contributes differentially to various cognitive and perceptual processes (Sperry, 1968; Sperry et al., 1969). The left hemisphere is inferred to play a larger role in verbal tasks, whereas the right hemisphere is more dominant in nonverbal and spatial tasks (Borod et al., 1992; Gazzaniga, 2000; Witelson and Pallie, 1973). Consistent with this, studies revealed that the right parietal cortex played a far more important role in spatial attention (Blumenfeld, 2002; Heilman and Van Den Abell, 1980). Lateralization is not limited to primates. Maternal mice have left hemisphere advantage in processing ultrasonic sounds emitted by pups (Ehret, 1987), and pup retrieval depends on the left but not the right auditory cortex (Marlin et al., 2015). In rats, it is suggested that there is a rightward bias of hippocampal functions in spatial memory storage and retrieval (Klur et al., 2009). Thus, despite the apparent symmetric appearance of mammalian brains, one hemisphere can play functionally more important roles.

What causes certain sensory, motor, and cognitive functions to be lateralized in one hemisphere? The biological basis of this asymmetry remains elusive. Multiple factors including evolution, genetic traits, and the interplay between early-on sensory experience (learning) and brain development are implied in lateralized brain functions (Michel et al., 2016; Sun and Walsh, 2006). Studies in humans reveal lateralized network activity that is probed using fMRI, which uses blood flow to assess brain activity (Nielsen et al., 2013; Pool et al., 2014; Price, 2010). However, few studies have probed the causal contribution of these activities to behavior. The mouse is a genetically tractable organism, allowing area-specific perturbation at high spatial and temporal resolution (Deisseroth, 2015; Luo et al., 2018). We wish to take advantage of the genetic tools to probe whether short-term memory (STM), a cognitive process that bridges past sensory stimuli with future actions (Jonides et al., 2008), can be lateralized in one hemisphere, and if so, how the left and right hemispheres can interact to produce this asymmetry.

STM plays a vital role in almost every cognitive process, including working memory, decision making, and reasoning (Baddeley and Hitch, 1974; Jonides et al., 2008). Neural correlates of STM (i.e., persistent activity) have been recorded from multiple brain areas, including the prefrontal cortex, parietal cortex, premotor cortex, motor cortex, thalamus, basal ganglia, and cerebellum in multiple species including primates and rodents (Erlich et al., 2011; Esmaeili et al., 2021; Funahashi et al., 1989; Fuster and Alexander, 1971; Gallero-Salas et al., 2021; Gao et al., 2018; Gilad et al., 2018; Goard et al., 2016; Guo et al., 2014b, 2017; Hanks et al., 2015; Inagaki et al.,

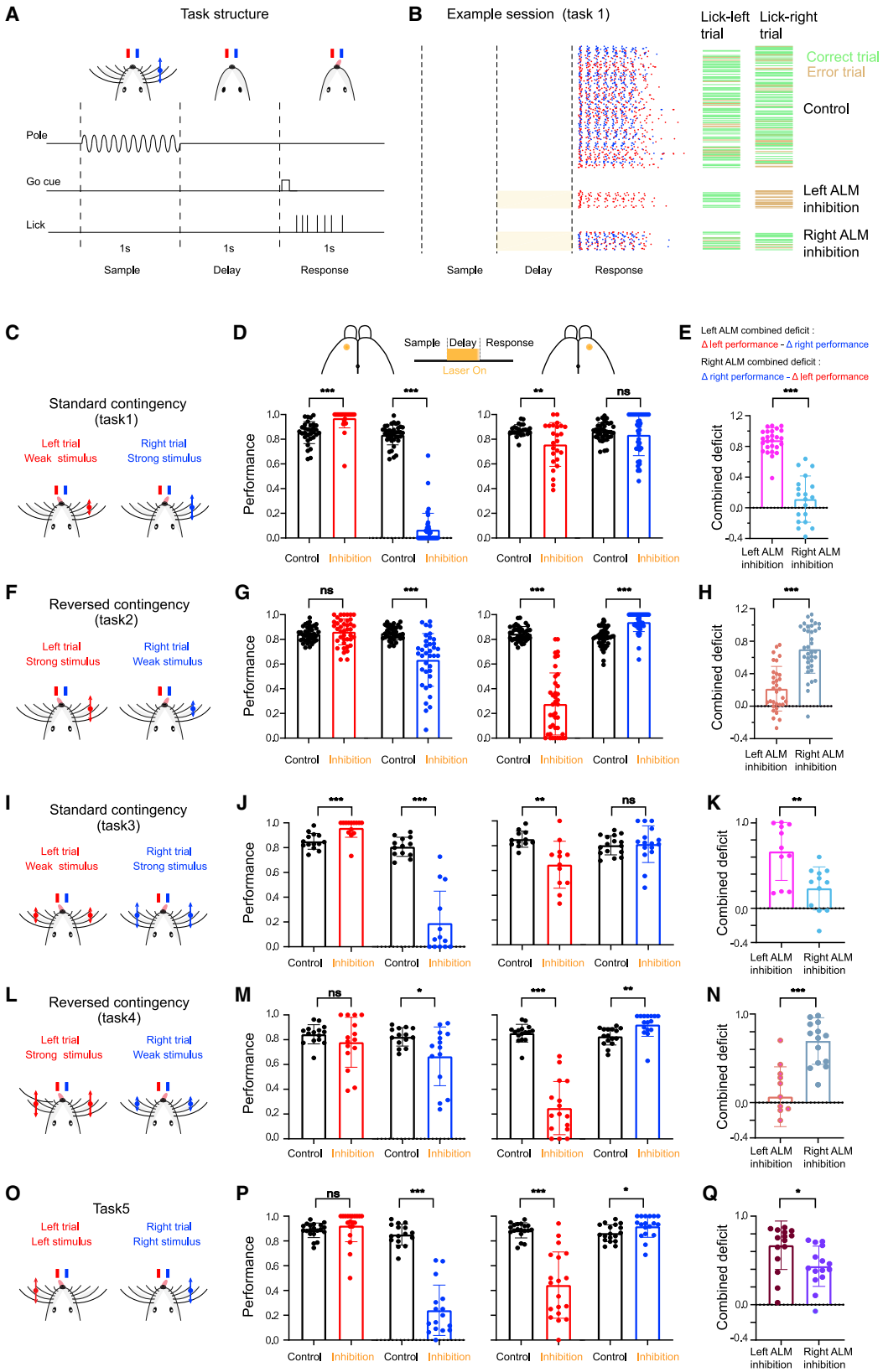

(legend on next page)

2019; Kopec et al., 2015; Mayrhofer et al., 2019; Romo et al., 1999; Tanji and Evarts, 1976; Wu et al., 2020). In a tactile-based decision-making task, optogenetic inhibition targeted to the delay period identified the anterior lateral motor cortex (ALM, part of frontal cortex) as a crucial area for STM (Guo et al., 2014b). A large fraction of ALM neurons exhibits persistent activity predicting future licking directions (Guo et al., 2014b; Li et al., 2015). Thus, persistent activity during the delay period also represents motor planning, a prospective form of STM (Svoboda and Li, 2018). Persistent activity has a distributed nature involving a network of brain regions (Christophel et al., 2017; Svoboda and Li, 2018). Persistent activity in ALM depends on thalamocortical reciprocal projections (Guo et al., 2017), is specifically shaped by the cortico-basal ganglia-thalamo-cortical loop (Wang et al., 2021), and is disrupted by stimulation of the fastigial nucleus of cerebellum (Gao et al., 2018). In addition to subcortical inputs, ALM also receive intense projections from the contralateral ALM. Persistent activity in ALM resists brief optogenetic inhibition, and this robustness depends on the recovery signal from the contralateral ALM (Li et al., 2016). A recent study further demonstrated that activity in ALM can be vulnerable to perturbation if frontal networks are not modular across hemispheres (Chen et al., 2021). Thus, ALM is a cortical circuit hub for STM.

Here, we ask whether the left and right ALM contribute equally to STM. And if the left and right ALM contribute asymmetrically to STM, what is the underlying circuit mechanism? To answer these questions, we developed five versions of the tactile-based decision-making task (known as "five tasks" hereafter) and discovered that the left and right ALM contributed differently to STM in a task-dependent way, with either the left, right, or both ALM playing crucial roles (i.e., being dominant). In contrast to intuition, neural activity in the left and right ALM was similar, independent of the side that was playing a dominant role. By combing electrophysiology with optogenetic inhibition, we showed that the dominant ALM strongly regulated STM activity in the non-dominant ALM, but not vice versa. This asymmetric interaction predicted inhibition deficits across sessions, animals, and tasks, suggesting that it is one important factor influencing functional lateralization.

RESULTS

Differential contribution of the left and right ALM to STM

Mice performed a tactile-based decision-making task with a STM component (Figures 1A, S1A–S1D) (Guo et al., 2014b; Wang et al., 2021). During the sample epoch, mice discriminated the strength of the vibration using their whiskers (strong stimulus, 1,838°/s peak velocity; weak stimulus, 408°/s). During the subsequent delay epoch (i.e., STM epoch), mice maintained the tactile experience in the brain and planned a directional licking. Following an auditory "go" cue, mice reported the stimulus strength with directional licking (left or right). Mice withheld licking during the sample and delay epoch, and the rate of licking before the response cue was low (Figures 1B and S1D). The correct response led to a reward (~4 μL milk, strong stimulus → right water spout, weak stimulus → left water spout, for the standard contingency; Figure 1C). Mice discriminated weak and strong stimuli with high accuracy (performance 85.4% ± 0.6%, mean ± SEM; Figure 1D).

To check whether the left and right ALM play different roles, we performed optogenetic inhibition during the STM period. Inhibition was achieved by activating parvalbumin (PV) GABAergic interneurons in PV-ReaChR transgenic mice with 594-nm laser illumination (Li et al., 2019). Photoinhibition of the left ALM significantly reduced task performance in lick-right trials (defined according to whisker stimulation strength) and increased performance in lick-left trials (t test, $p < 0.001$ for both conditions; Figure 1D), producing an ipsilateral bias consistent with previous findings (Guo et al., 2014b; Li et al., 2015). Inhibition of the right ALM affected task performance little in lick-right trials, while it produced a small but significant reduction in lick-left trials (lick-right trial, −2.6% ± 2.9%, $p = 0.70$; lick-left trial, −11.5% ± 3.5%, $p < 0.01$; mean ± SEM, t test; Figure 1D). Inhibition of the left ALM produced a much larger behavioral deficit compared with the right ALM (combined deficit in both trial types, left ALM versus right ALM, 88.1% ± 3.1% vs 11.4% ± 6.7%, $p < 0.001$; mean ± SEM, t test; Figure 1E; Method details). Thus, the left ALM plays a much larger role in STM (i.e., the left ALM dominates).

Figure 1. Differential contribution of the left and right ALM to STM

(A) Task structure.

(B) Example behavioral session. Each dot represents a lick; red, left licks; blue, right licks. Right horizontal lines show trial outcomes. Shading denotes trials with the left or right ALM inhibition.

(C) Schematic of the task under the standard contingency. Mice learn to associate the strong (weak) stimulus with licking the right (left) water spout.

(D) Optogenetic inhibition of the left but not right ALM during the delay epoch produces a large behavioral deficit. Each dot represents a session (59 sessions from 13 mice). Data points with at least 10 photoinhibition trials are shown. Data are represented as means ± SDs. *$p < 0.05$, **$p < 0.01$, ***$p < 0.001$, 2-tailed t test.

(E) Combined deficit to quantify the ipsilateral bias during the left or right ALM inhibition.

(F) Schematic of the task under the reversed contingency. Mice learn to associate the strong (weak) stimulus with licking left (right) water spout.

(G–H) Same format as in (D) and (E), but for the reversed contingency (73 sessions from 11 mice). Inhibition of the right but not left ALM produces a large behavioral deficit.

(I) Schematic of the task with bilateral tactile input under the standard contingency. Relevant to (J) and (K).

(J–K) Same format as in (D) and (E) (16 sessions from 6 mice), but for task 3. Inhibition of the left but not right ALM produces a large behavioral deficit.

(L) Schematic of the task with bilateral tactile input under the reversed contingency. Relevant to (M) and (N).

(M and N) Same format as in (D) and (E) (18 sessions from 4 mice). Inhibition of the right but not left ALM produces a large behavioral deficit.

(O) Schematic of the task with symmetric sensory-motor associations. Stimulation of whiskers in the left (right) side is associated with licking the left (right) spout. Relevant to (P) and (Q).

(P and Q) Same format as in (D) and (E) (22 sessions from 5 mice). Inhibition of the left and right ALM produces a more symmetric pattern of deficits.

See also Figures S1 and S2.

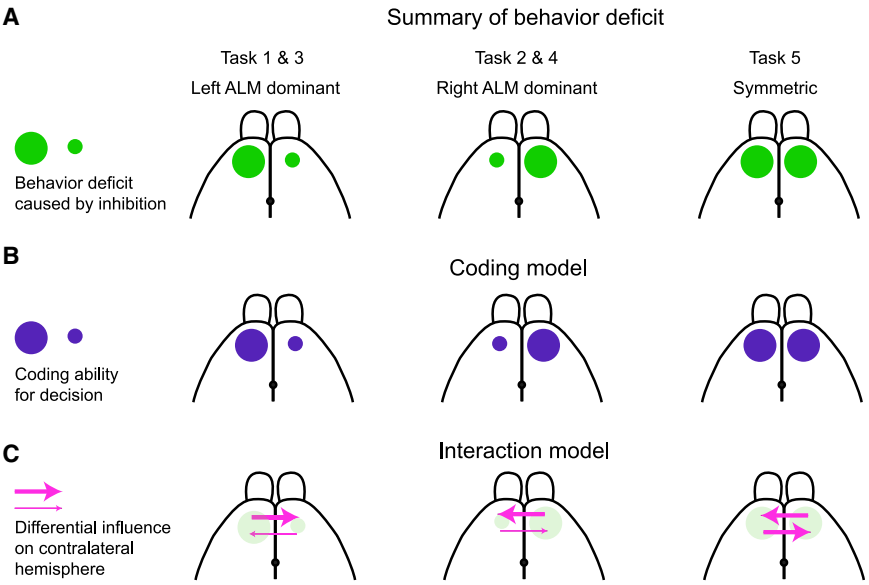

Figure 2. Hypothesis to explain the differential behavioral deficits

(A) Summary of behavioral deficits caused by ALM inhibition in different tasks. Dot size encodes for the magnitude of behavioral deficit.

(B) In hypothesis 1, neurons in the dominant hemisphere (left ALM for tasks 1 and 3 and right ALM for tasks 2 and 4) have a higher encoding ability of upcoming choice compared with neurons in the non-dominant hemisphere (right ALM for tasks 1 and 3 and left ALM for tasks 2 and 4).

(C) In hypothesis 2, the dominant hemisphere has a larger impact on the non-dominant hemisphere, but not vice versa.

To check whether the left hemisphere intrinsically dominates, we reversed the sensory-motor contingency (i.e., strong stimulus → left water spout, weak stimulus → right water spout) in a different batch of mice (Figures 1F and S1A–S1D). This strategy is commonly used to differentiate the sensory and motor components of brain functions (Chereau et al., 2020; Guo et al., 2014b; Pho et al., 2018). Under the reversed contingency, optogenetic inhibition of the right ALM produced a much larger combined deficit (right ALM versus left ALM, 70.2% ± 4.9% versus 21.5% ± 5.0%, $p < 0.001$; mean ± SEM, t test; Method details; Figures 1G and 1H), indicating that the right ALM dominates in the reversed contingency. Notably, mice on average did not prefer licking one spout during the task, and the licking latency was indistinguishable between lick-left and lick-right trials in either contingency (Figures S1B and S1E). We further confirmed that mice developed no bias throughout the early to late training, based on weights extracted from PsyTrack (Roy et al., 2021) (Figure S2). These results demonstrate that the left and right ALM are differentially involved in STM.

Differential contribution of the left and right ALM to STM with bilateral tactile inputs

Tactile information from whiskers on the right cheek is routed to the somatosensory cortex in the left hemisphere (Diamond et al., 2008). To check whether this could explain the phenomenon of dominance, we trained different batches of mice to perform another two versions of the task, during which mice received symmetric tactile stimulation (Figures 1I and 1L). Under the standard contingency (task 3), photoinhibition of the left or right ALM produced a similar pattern of behavioral deficits as in task 1 (Figures 1J and 1K), with the inhibition of the left ALM causing a much larger deficit (left ALM versus right ALM, 66.5% ± 9.5% versus 23.4% ± 7.0%, $p < 0.01$; mean ± SEM, t test; Figure 1K). Similarly, under the reversed contingency (task 4), photoinhibition of the left or right ALM produced a similar pattern of deficits as in task 2 (Figure 1M), with the inhibition of the right ALM producing a much larger deficit (right ALM versus left ALM, 69.6% ± 6.5% versus 6.6% ± 9.1%, $p < 0.001$; mean ± SEM, t test; Figure 1N). Thus, mice demonstrated similar dominance, independent of whether tactile information was unilateral or bilateral.

In tasks 1–4, the strength of stimuli is not equal in lick-left and lick-right trials. We posited that making the sensory-motor association completely symmetric may render the left and right ALM similarly involved in STM. To test this, we developed task 5, in which a strong stimulation of the left (right) side of whiskers predicted water reward from the left (right) lickport (Figure 1O). Photoinhibition of the left ALM significantly reduced task performance in lick-right trials, while inhibition of the right ALM significantly reduced task performance in lick-left trials (t test, $p < 0.001$ for both conditions; Figure 1P). Inhibition of the left ALM in lick-left trials and inhibition of the right ALM in lick-right trials increased performance (not significant for the left ALM, $p = 0.04$ for the right ALM; Figure 1P). Although the combined deficit was still different between the left and right ALM, the difference was much smaller compared with previous four tasks (differences in tasks 1−5: 76.7% ± 7.2%, 48.7% ± 6.5%, 43.2% ± 12.0%, 63.0% ± 11.8%, 23.7% ± 8.7%, mean ± SEM; task 5 versus tasks 1–4, $p < 0.001$, $p = 0.01$, $p = 0.1$, $p = 0.003$, bootstrap to count for variability across sessions and animals; Figure 1Q).

Thus, by varying sensory-motor associations, we have developed five versions of the tactile-based decision-making task with a STM component (Figure 1). By using temporal-precise optogenetic inhibition, we provide evidence that the left and right ALM play differential roles in STM in a contingency-dependent way, with the left ALM being dominant in the standard contingency (tasks 1 and 3), the right ALM being dominant in the reversed contingency (tasks 2 and 4), and both the left and right ALM playing important roles in task 5 (Figure 2A). As photoinhibition of the non-dominant ALM affected task performance little, we hypothesized that neurons in the non-dominant side may not encode trial-type information (i.e., neurons in the left and right ALM had different encoding capability; coding model; Figure 2B).

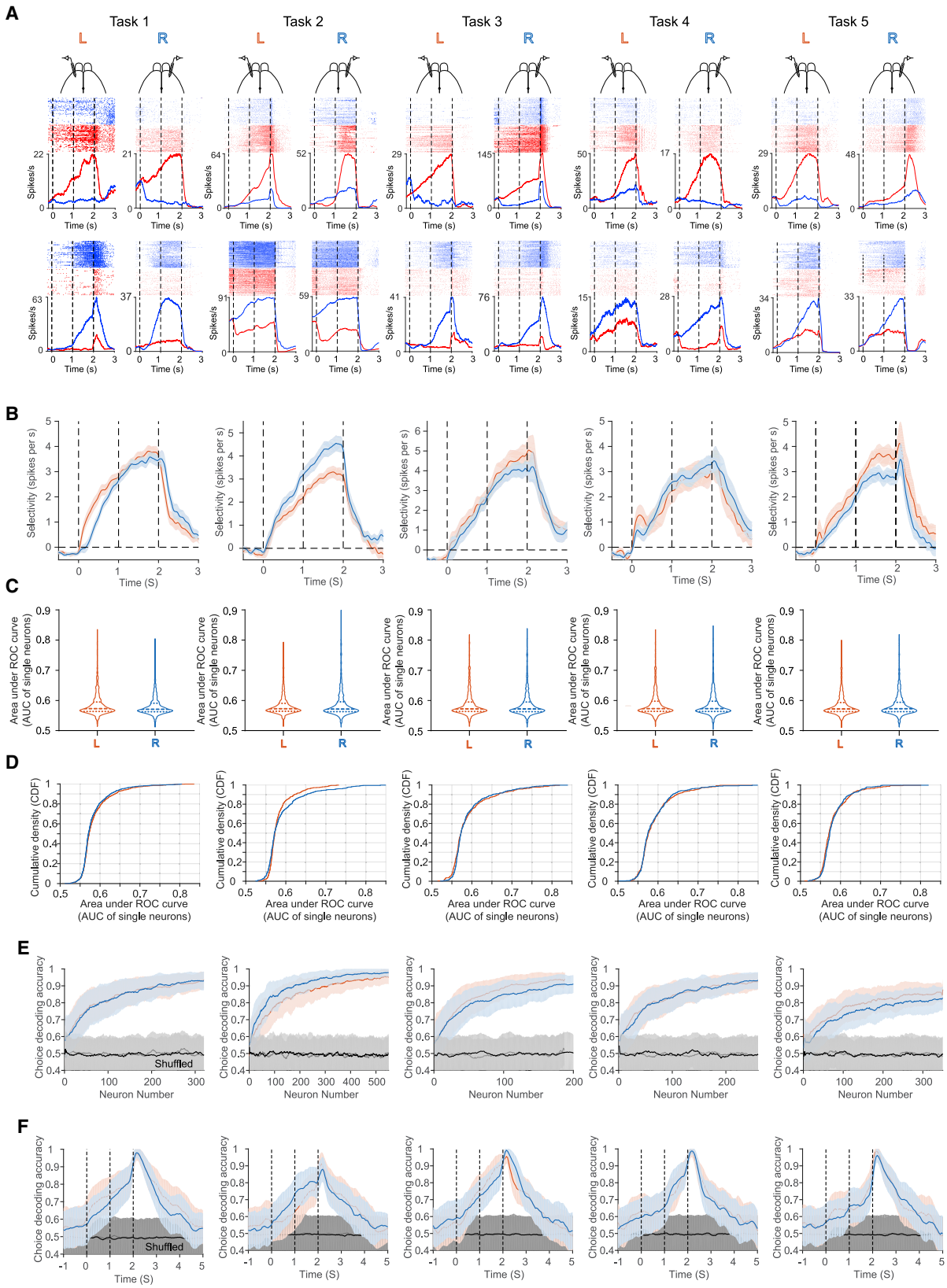

(legend on next page)

Alternatively, the differential effects may result from the distinct interaction patterns between the left and right ALM (interaction model, Figure 2C).

Similar neural activity and encoding capability in the left and right ALM

To test the coding model, we recorded 8,329 single units from the left and right ALM across tasks 1–5. In contrast to our prediction, neurons in either the left or right ALM under either the standard or reversed contingency differentiated trial types in the sample, delay, and response epochs (Figures 3A and S1F–S1N). There were similar fractions of selective neurons in the left and right ALM across tasks (Figures S1J and S1N). We further categorized neural activity profiles using hierarchical clustering (Finkelstein et al., 2021). There were similar fractions of neurons within each cluster for the left and right ALM across tasks (Figure S3). The selectivity, defined as the difference in firing rate between the preferred and non-preferred trials, ramped up in the sample and delay epochs, similarly in the left and right ALM under either contingency (Figure 3B).

We then checked how well single ALM neurons encode choice information. For each neuron, a balanced set of trials were randomly selected with equal proportions of lick-left correct, lick-left error, lick-right correct, and lick-right error trials. Delay-epoch activity predicted upcoming choice (licking the left or right spout) with variable accuracy (characterized by area under receiver operating characteristic curve [AUC]; Figure 3C). The distribution was overall similar for neurons in the left and right ALM across tasks (Figures 3C and 3D). We further randomly selected a pseudo-population of neurons and trained a support vector machine (SVM) classifier with 10-fold cross-validation (Wang et al., 2021). The accuracy of the classifier increased with the number of randomly selected neurons, similarly between the left and right ALM across tasks (Figure 3E). We then randomly selected 200 neurons to examine how the decoding accuracy evolved with trial progression. Choice information gradually increased from the sample to the delay epoch and reached a peak at the beginning of the response epoch, similarly for neurons in the left and right ALM (Figure 3F). Thus, neurons in the left and right ALM have similar response pattern and encoding capability across tasks at both single-neuron and pseudo-population levels.

Neural population dynamics in the left and right ALM

ALM population dynamics encodes upcoming choice in single trials with high accuracy (Li et al., 2016). To check whether population dynamics predicted upcoming choice consistently across hemispheres, we performed simultaneous population recordings bilaterally using NeuroPixel probes in tasks 3–5 (Figure 4A). We constructed a linear decoder by projecting population activity along the coding direction (CD, the direction that maximally separated lick-left and lick-right population trajectories) and comparing trajectory endings with the decision boundary (DB; Method details) (Li et al., 2016). Decoding using this dimensionality reduction technique revealed that both hemispheres encoded upcoming choice consistently in most of trials (dots in the upper right and lower left quadrants; Figures 4B and S4A). When both hemispheres agreed in prediction, most of the trials were correct (filled dots in Figure 4B; see Figure S4C for predictions broken up in correct left trials, error left trials, correct right trials, and error right trials). In error trials, the portion of consistent predictions was significantly lower (task 3, $p = 0.01$, task 4, $p = 0.01$, task 5, $p < 0.0001$; paired t test, Figure 4C). We further examined conflict trials when both hemispheres disagreed, with only one side predicted correctly, and found that both the left and right ALM had a similar fraction of correct predictions (Figure 4D). Thus, in single trials, ALM population activity predicted upcoming choice similarly across hemispheres, independent of which side dominated.

We further characterized co-fluctuations between pairs of neurons (i.e., noise correlation, NC). NC can reflect shared input as well as functional connectivity between pairs of neurons (Cohen and Kohn, 2011). Neurons in either the left or right ALM or across hemispheres had higher NCs compared with shuffled trials (Figure 4E). The distribution of NCs was wider than that in shuffled data (pooled data across sessions, Figure 4F). NC was positively correlated with signal correlation (the Pearson correlation of mean activity, Figure 4G). NCs within ALM and across hemispheres was small (Figures 4H–4J). The NCs within right-preferring neurons and left-preferring neurons were positive, while the NC between the two response groups of neurons was negative or close to zero. The phenomenon of dominance cannot be explained by the difference in mean NCs as the difference between the left and right hemispheres was not significant (Figures 4H–4J).

Figure 3. Neurons in the left and right ALM have similar selectivity and encoding capability

(A) Peristimulus time histogram (PSTH) of example neurons from the left ALM (left column) and right ALM (right column) for 5 tasks. Top row, example left-preferring neurons; bottom row, example right-preferring neurons. Spike raster is shown on the top of each panel. Red, lick-left trials; blue, lick-right trials. Time is aligned to the sample start.

(B) Mean selectivity (the firing rate difference between the preferred and non-preferred trials) for delay-selective neurons. The left (light red) and right (light blue) ALMs have a similar pattern of selectivity. Significance is determined by comparing the selectivity during the delay epoch using the t test ($p = 0.45$, 0.006, 0.48, 0.74, and 0.14 for tasks 1–5, respectively). Shading denotes SEM. There are 965, 435, 343, 323, and 338 selective neurons under tasks 1–5, respectively.

(C) Violin plot of the decoding accuracy of choice for single neurons (see Method details). The color scheme is the same as in (B).

(D) The cumulative density function (CDF) of decoding accuracy has a similar trend across hemispheres ($p = 0.17$, 0.02, 0.15, 0.91, and 0.28 for tasks 1–5, respectively. p value is determined by 2-sample Kolmogorov-Smirnov test; same data as in C).

(E) The accuracy of choice decoding increases with the number of randomly selected neurons in tasks 1–5 (Method details). Black lines, trials shuffled. Shading denotes SEM. $p = 0.61$, 0.46, 0.87, 0.87, and 0.86 for tasks 1–5, respectively (bootstrap, Method details).

(F) The accuracy of choice decoding evolves with trial progression. Step size, 50 ms. Window size, 100 ms. Two hundred neurons are randomly selected (Method details). $p = 0.68$, 0.02, 0.06, 0.63, and 0.83 for tasks 1–5, respectively (bootstrap, Method details).

See also Figure S3.

CellPress
OPEN ACCESS

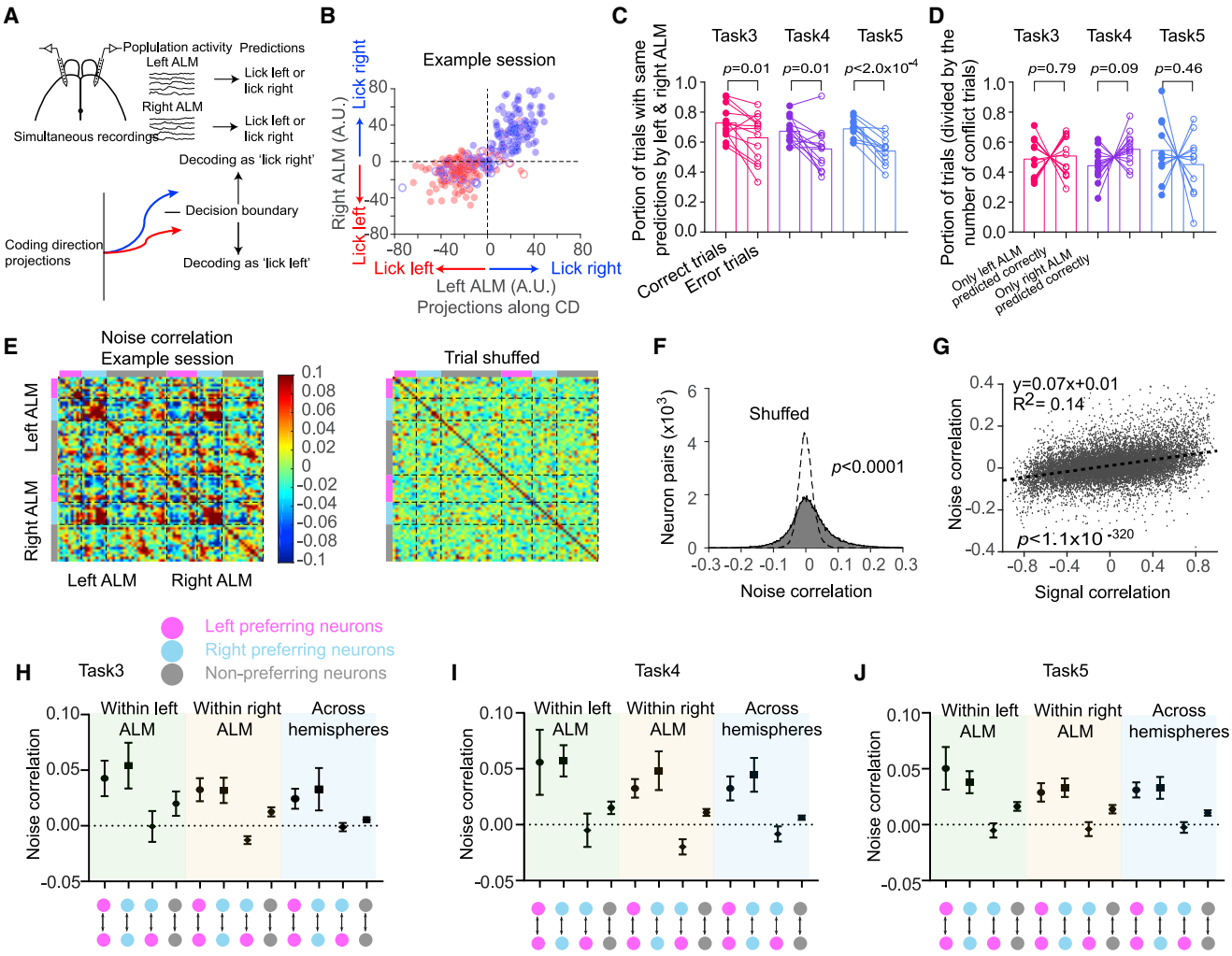

Figure 4. Neural correlation across hemispheres probed with simultaneous bilateral recordings

(A) Schematic of decoding using population activity on single trials. Neural trajectory is projected along the coding direction (CD) that is determined for each hemisphere separately. A linear decoder is constructed by comparing trajectory endings with the decision boundary (Method details).

(B) CD projection values at the end of delay epoch in an example session (see Figure S4 for more example sessions). Blue circles, lick-right trials according to whisker stimulation strength. Red circles, lick-left trials. Filled circles, correct trials; open circles, error trials.

(C) Portion of trials with same predictions based on CD projection values across hemispheres. The fraction of same predictions in correct trials is significantly higher than in error trials. Each line represents a session (13, 13, and 11 sessions for tasks 3–5, respectively). Significance is determined using paired t test.

(D) Portion of trials with conflict predictions across hemispheres.

(E) Noise correlation of simultaneously recorded neurons in an example session. Right panel, trials shuffled.

(F) Distribution of noise correlations (data from all neural pairs are included). Dotted lines, trials shuffled. p value is determined by bootstrap.

(G) Noise correlation increases with signal correlation. Dashed line, linear fitting.

(H–J) Noise correlation within hemisphere or across hemispheres in tasks 3–5 ($p > 0.05$, bootstrap, for all response groups between 2 hemispheres). Data are represented as means ± SDs.

See also Figure S4.

Differential effect of ALM inhibition on neural activity in the contralateral hemisphere

To test the interaction model, we recorded neural activity from both hemispheres with unilateral optogenetic inhibition (Figure 5). As CD projected activity predicted upcoming choice with high accuracy (Figures 4B, 4C, and S4), we checked how unilateral inhibition affected CD projected activity in the contralateral hemisphere (Figures 5B and 5C). Inhibition reduced the separation of neural trajectories in different sessions variably (Figure 5B). We defined the separation in the last 200 ms of the delay period as residual separation. In tasks 1 and 3 (standard contingency), inhibition of the left ALM caused a larger behavioral deficit, and accordingly resulted in smaller residual separations compared with the right ALM inhibition (Figure 5C). In tasks 2 and 4 (reversed contingency), inhibition of the right ALM caused a larger behavioral deficit and a

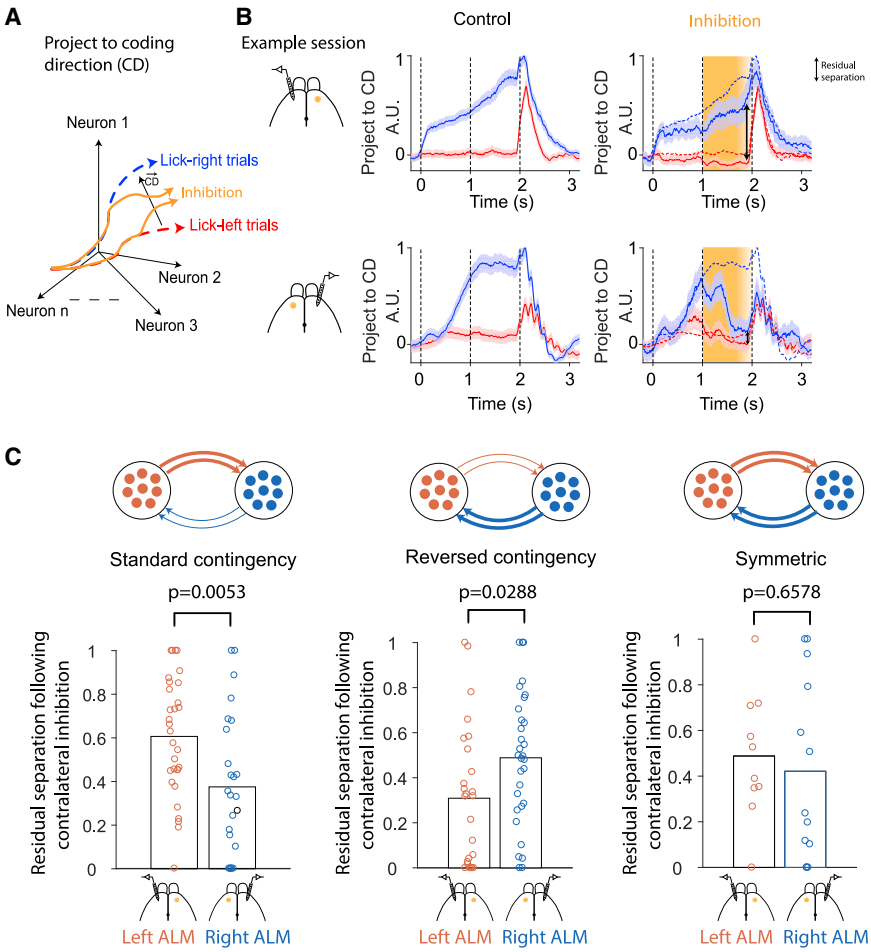

Figure 5. The dominant hemisphere is more resistant to contralateral inhibition

(A) Schematic of neural trajectories projected along CD. During contralateral inhibition, the separation between lick-left and lick-right trials is reduced.

(B) An example session from task 1 showing differential resistances to contralateral inhibition. Top row, contralateral inhibition influences projections along CD little; bottom row, trajectories collapse during contralateral inhibition. Shading, SEM estimated using bootstrap. Dashed lines from the control were superimposed for comparison.

(C) Residual separation during contralateral inhibition across tasks (normalized by the control separation). Each dot denotes a session. p value is determined using t test. The dominant hemisphere is more resistant to contralateral inhibition and has a larger impact on the contralateral hemisphere. For task 1, n = 4 mice for the left ALM recording and n = 7 for the right ALM. For task 2, n = 7 for both ALMs. For tasks 3–5, n = 4 for both ALMs.

See also Figures S4 and S5.

larger effect on contralateral activity (Figure 5C). In task 5, inhibition of the left and right ALM affected contralateral activity similarly. Thus, inhibition of the dominant and non-dominant ALM differentially affects STM activity in the contralateral hemisphere.

We further checked how unilateral inhibition affected the coding capability of neural activity in the contralateral hemisphere. We used the same decoder as in Figure 4 and calculated the decision boundary using control trials (Figure 6A). Neural activity in either the left or right ALM predicted upcoming choices well during control, as manifested by the steep curves in Figures 6B and 6C. Unilateral inhibition of the dominant ALM (left ALM in tasks 1 and 3, right ALM in tasks 2 and 4, the left and right ALM in task 5) strongly affected behavioral performance (Figure 1), and accordingly, this perturbation dramatically reduced the encoding capability in the contralateral hemisphere (see more flat curves in Figures 6B and 6C, difference between control and perturbation in Figure 6D, and schematic in Figure 6E). On the contrary, when perturbation caused less behavioral effect, its effect on the coding capability was also smaller (Figures 6B and 6C). In task 5, the mean difference from control was large in both hemispheres (Figure 6D), consistent with the fact that inhibition of either hemisphere affected performance (Figures 1O–1Q). Despite this, the right ALM exhibited a significantly larger difference, consistent with the larger behavioral deficit caused by the left ALM inhibition (Figures 1O–1Q). These results indicate that the left and right ALM have distinct interactions across tasks and support the interaction model (Figure 2C).

We noticed that laser illumination dramatically increased the activity of putative fast-spiking neurons and almost completely silenced activity of putative pyramidal neurons (Figures S4D–S4G). In the hemisphere that was not directly illuminated by the laser, activities of both putative fast-spiking and pyramidal neurons were slightly reduced, which indicated that laser light did not directly influence the contralateral hemisphere (Figure S4E). Although inhibiting one hemisphere only slightly reduced the mean activity of the contralateral hemisphere, many neurons showed significantly increased or decreased activities (Figures S5A–S5C). The fraction of significantly modulated neurons was similar between the left and right ALM across tasks 1–5 (Figure S5C). The amplitude of modulation followed a similar relation with baseline activity in the left and right ALM across tasks 1–5 (Figure S5D). These results indicate that the differential influence on the contralateral hemisphere cannot be simply attributed to changes at the level of individual neurons.

Prediction of behavioral deficits based on ALM activity following unilateral inhibition

Unilateral inhibition of ALM during the delay epoch impaired upcoming choice variably across five tasks (Figure 1). To understand this variability, we checked whether the magnitude of behavioral deficits could be predicted based on how perturbation affected contralateral activity (Figure 7A). We classified

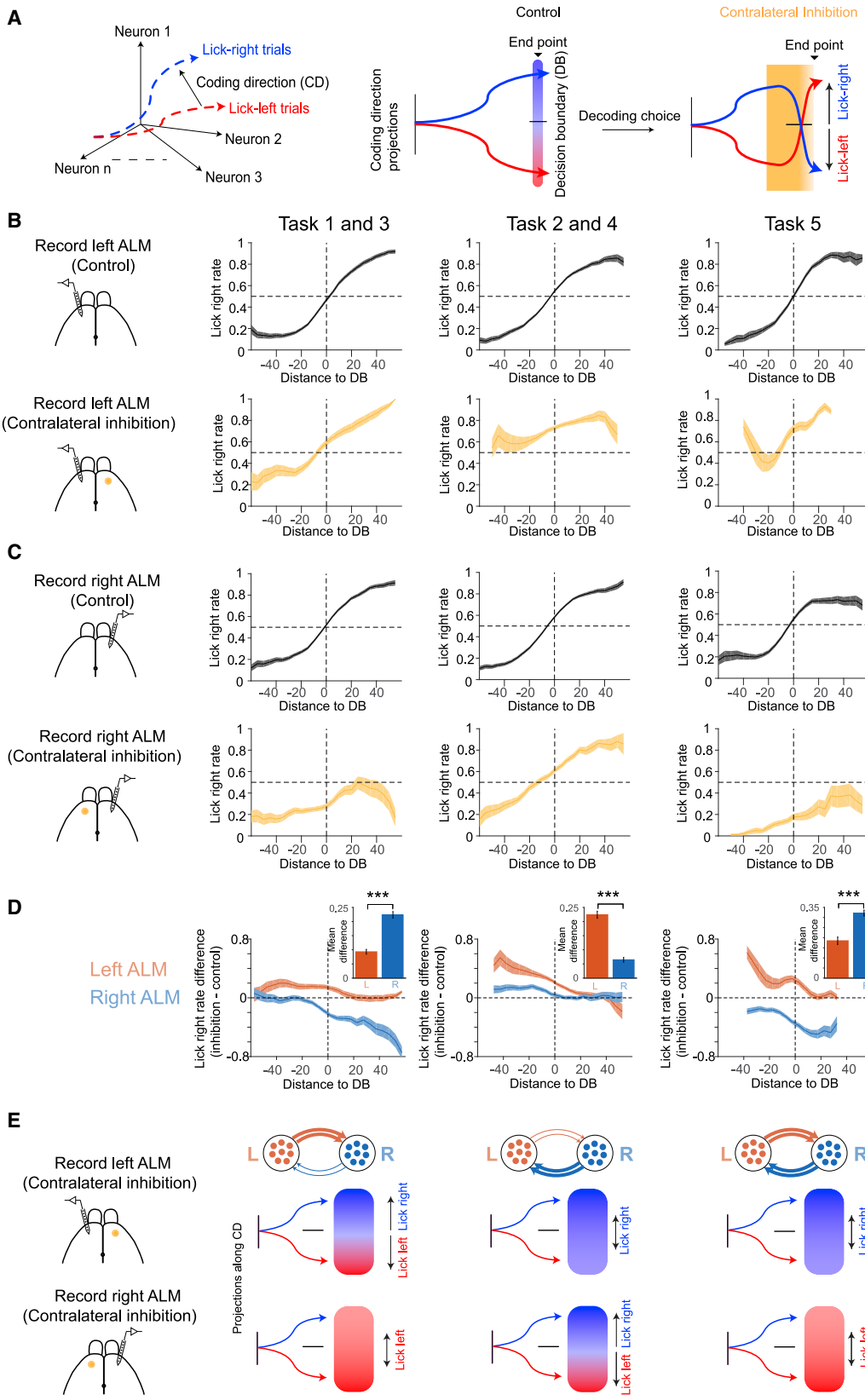

(legend on next page)

sessions based on behavioral deficits into sessions with small and large performance changes (Figure 7B). In sessions with small performance change, inhibition affected neural trajectories little, while in sessions with large performance change, trajectory endings were evidently shifted compared with the control (Figures 7C and 7D). We quantified the influence on contralateral hemisphere by calculating the distance of the projection distribution between control and inhibition trials (see Method details). Influence on the contralateral hemisphere correlated well with behavioral deficits in individual sessions and individual mice (data pooled from tasks 1–5; Figures 7E and 7F). This evident correlation also held when we performed the same analysis for sessions and mice in individual tasks (Figure S6). When we pooled data from individual animals for each task, the influence on contralateral activity explained an even larger portion of performance change (Figure 7G). This analysis indicates that influences on contralateral hemisphere and behavior deficit were coupled with each other (Figure 7H). Thus, even though the left and right ALMs play differential contributions to STM, the variable behavioral deficits across sessions, animals, and tasks can be predicted by the degree of perturbation on the contralateral hemisphere.

Relation between orofacial movements and ALM activity

Body movements account for a considerable fraction of variabilities in neural activity (Esmaeili et al., 2021; Gilad et al., 2018; Musall et al., 2019; Stringer et al., 2019). We wonder whether body movements contribute to the variable behavioral deficits we observed. To check this, we used two high-speed cameras to capture the side and bottom views of orofacial movements during photoinhibition in a subset of mice performing task 1 (Method details). The jaw, whisker pad, and nose of mice exhibited variable movements across trials (Figures S7A and S7B). We characterized these movements using motion energy (ME) that was the absolute difference between consecutive video frames (Mayrhofer et al., 2019; Musall et al., 2019; Stringer et al., 2019). ME was variable across trials, with the mean ME of jaw and whisker pad larger in lick-right trials (Figure S7C). To check whether neural activities in ALM were causally related to movements, we unilaterally or bilaterally inhibited ALM during the delay epoch. ME during inhibition remained at a similar level as in the control, indicating that orofacial movements during the delay epoch were largely independent of ALM activity (Figures S7D and S7E). We then wondered whether movements could predict neural activity along CD, the subspace of population activity that encoded upcoming choice. CD projected activity in high and low ME trials was similar in most sessions and there was no significant correlation between ME and the projected activity across trials in individual sessions (Figures S7F and S7G; 68% sessions had $p > 0.05$). Furthermore, ME only explained a small fraction of variations of CD-projected neural activity (78% sessions had $R^2 < 0.1$). These results revealed that the choice-encoding subspace during the delay epoch is largely independent of orofacial movements. Consistently, the choice-encoding and movement-encoding subspaces are near-orthogonal to one another in ALM (Inagaki et al., 2022), and ALM shows sustained activity predicting upcoming licking even after preparatory movements are accounted for (Esmaeili et al., 2021). We also inspected ALM activity in quiet trials and found that there was a robust increase of neural activity during STM even in these quiet trials (Figure S7H). Thus, during STM, the orofacial movements are largely independent of ALM activity, and the inhibition of ALM does not affect these movements, indicating that the variable orofacial movements are not responsible for the variable behavioral deficits.

DISCUSSION

The left and right ALMs presumably play a similar role in untrained mice. However, their contribution to STM can be adjusted to exhibit dominance in one side or to be equipotent in both sides (Figure 1). This not only cautions us that small task modifications can qualitatively affect the lateralization of brain functions but also suggests that the investigation of cognitive functions should not only focus on one hemisphere. The phenomenon of dominance may suggest that the non-dominant ALM had less STM-related activity. In contrast to this assumption, neural activity in both hemispheres exhibit similar dynamics and encoding capability, despite that one hemisphere only plays a minimal role during STM (Figures 3 and 4). The difference between the dominant and non-dominant hemispheres lies in their ability to influence the contralateral hemisphere (Figures 5 and 6). The dominant hemisphere is more independent and has a greater ability to gate the influence from the contralateral hemisphere, while the non-dominant hemisphere is more vulnerable to the input from the contralateral hemisphere. In addition, the

Figure 6. Differential effect on the coding ability of choice by contralateral inhibition

(A) Schematic of choice decoding during contralateral inhibition. The decision boundary (DB) is determined from control trials (same as in Figure 4A). The DB is further used to decode choices for trials with contralateral inhibition.

(B) The lick-right rate rises as distance to DB increases in control trials (top row), which means that the prediction accuracy improves with the increase in distance to DB. With contralateral inhibition, the ability to decode upcoming choices is largely preserved in tasks 1 and 3, but not in tasks 2, 4, and 5 (bottom row). Recordings were performed in the left ALM. Shading, SEM.

(C) Similar to (B), but for recordings in the right ALM. After contralateral inhibition, the steep trajectory is largely preserved in tasks 2 and 4, but not in tasks 1, 3, and 5.

(D) Quantification of deviation in decoding curves between the control and inhibition conditions. Significance is determined by bootstrap (***$p < 0.001$). Data are represented as means ± SEMs.

(E) Summary of the differential influence following contralateral inhibition. The dominant hemisphere (the left ALM in tasks 1 and 3; the right ALM in tasks 2 and 4) is minimally influenced by contralateral inhibition of the non-dominant hemisphere, but not vice versa. Inhibition of the dominant hemisphere biases mice to lick ipsilaterally, regardless of the distance of projected trajectory to DB (lick-left in tasks 1 and 3; lick-right in tasks 2 and 4). For task 5, inhibition of either hemisphere destroys the coding ability in the contralateral hemisphere.

See also Figure S5.

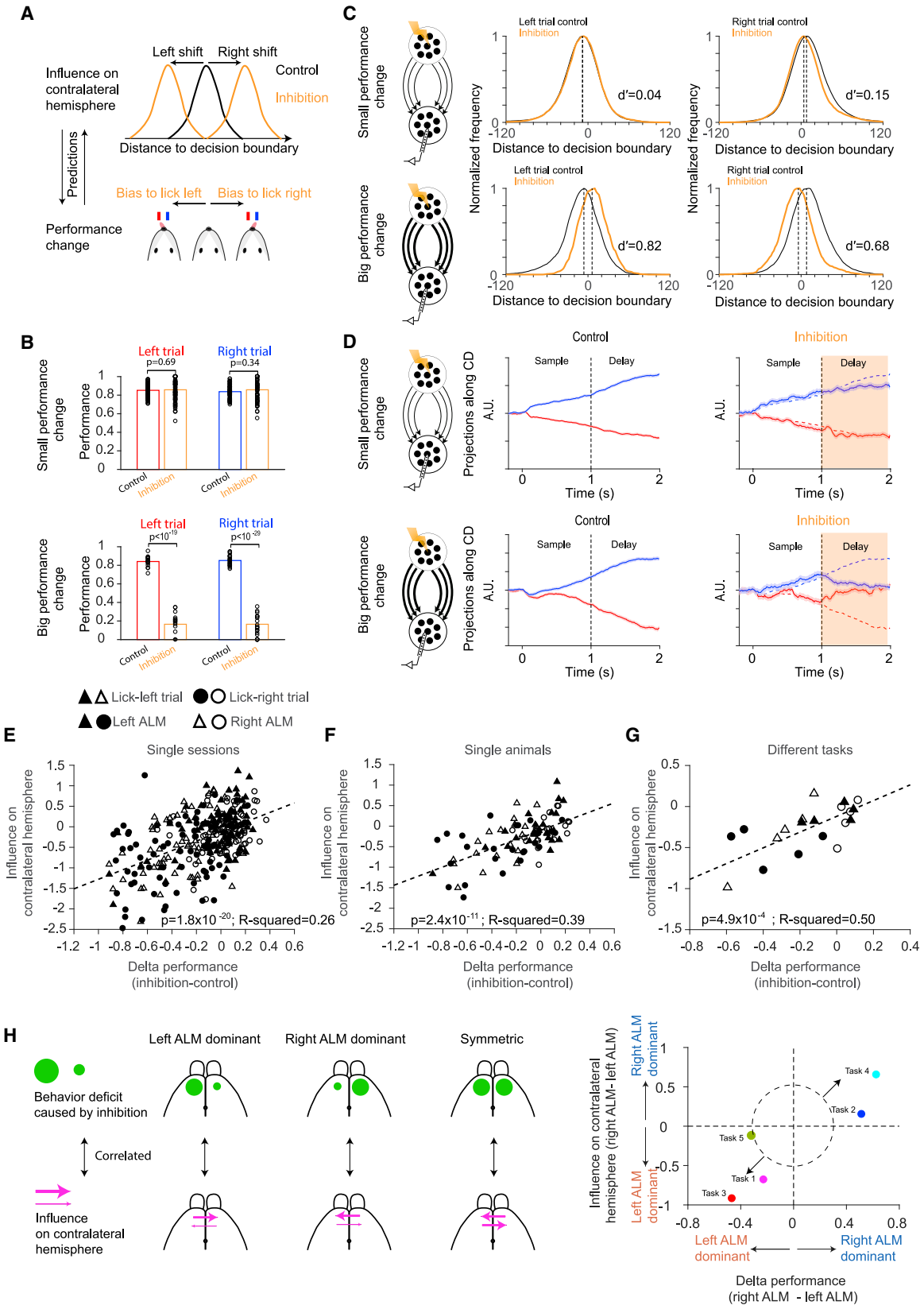

(legend on next page)

direction of coupling can be switched by changing sensory-motor contingency and tuned by the varying strength of the bilateral sensory input (Figures 1, 5, and 6). Furthermore, variations regarding the interaction pattern exist in different sessions, animals, and tasks. Remarkably, these distinct interactions across hemispheres are highly correlated with behavioral deficits caused by unilateral inhibition (Figure 7).

Possible origins of hemispheric dominance in different tasks

The phenomenon of hemispheric dominance in our tasks does not depend on whether sensory input is unilateral or bilateral (Figure 1). Mice do not have a preference of licking of either water spout (Figures S1 and S2). Multiple factors may contribute to the functional lateralization.

As the dominant ALM is always contralateral to the choice associated with the strong stimulus, this may reflect that mice strategically pay more attention to the salient stimulus. Consistent with this, both the left and right ALM are important in a task in which both whisker stimuli are equal in strength and presumably require similar attention (Figures 1O–1Q). However, the salience of stimuli is unlikely to be the sole factor as one hemisphere can still dominate with similar sensory input. In an auditory frequency discrimination task in which the sound pressure was fine-tuned to match response sensitivity, inhibition of the right ALM produced a much smaller behavioral deficit (Inagaki et al., 2018). We found similar results in task 5 (i.e., inhibition of the left ALM produced a much larger behavioral deficit compared with inhibition of the right ALM) (Figure 1P). These results may imply that there exists some intrinsic dominance, and mice preferentially choose the left ALM to maintain STM.

The above factors (different stimulus intensities and the possible intrinsic dominance) are the same within each task and thus alone cannot explain within-task variations among sessions and animals (Figure 7). The origin of these variations remains largely elusive. The brain is organized in a highly redundant network (Chen et al., 2021; Christophel et al., 2017). Dysfunction of one brain area can be compensated by other brain areas (Fridman et al., 2004; Frost et al., 2003; Li et al., 2016; Liu and Rouiller, 1999). ALM interacts with multiple sensory and motor areas (Esmaeili et al., 2021; Mayrhofer et al., 2019). The difference in the level of redundancy and compensation within animals may contribute to variable deficits following perturbation. In addition, differences in behavioral strategy adopted by mice can affect the relative contribution of frontal and posterior cortex to STM (Gallero-Salas et al., 2021; Gilad et al., 2018). Involvement of the prefrontal cortex for working memory storage can be shifted between the two hemifields following a change in instructed saccade direction (Brincat et al., 2021). Although the relative contribution of these factors to functional lateralization remains unknown, the asymmetric interactions between the left and right ALM could explain a large fraction of behavioral deficits, providing one crucial factor underlying the hemispheric dominance (Figure 7).

Possible benefits of functional lateralization

The benefits of functional lateralization remain largely unknown (Hartwigsen et al., 2021). It is thought that this organization can improve efficiency, increase the brain capacity, and avoid conflicting decisions between the two hemispheres (Rogers et al., 2004; Vallortigara, 2006; Vallortigara and Rogers, 2005). Research in artificial intelligence (AI) has shown that properly assigning different importance to multiple relatively independent networks can reduce catastrophic forgetting, an undesirable property commonly observed in continual learning (Aljundi et al., 2017; Rusu et al., 2016). The left and right hemispheres can function independently, and at the same time, they can also communicate with one another mainly through the corpus callosum, which may be beneficial for learning multiple tasks. Understanding functional lateralization may help design next-generation brain-inspired AI (Hartwigsen et al., 2021).

Relation to lateralization of other functions

Lateralization is not always fixed to one side of the brain. Humans typically develop hand usage preference (i.e., the preference for using the right or left hand for skillful movements). Approximately 95% of the right-handed population and 70% of the left-handed population have language ability dominant in the left hemisphere (Corballis, 2003). The neural mechanism of handedness is not completely understood and how handedness is developed is not yet clear (Nielsen et al., 2013; Pool et al., 2014; Sun and Walsh, 2006). Multiple factors, including

Figure 7. Behavioral deficit is linearly correlated with influence on the contralateral hemisphere

(A) Schematic to show the strategy to correlate influence on contralateral hemisphere and performance change. Influence on contralateral hemisphere is measured by the shift of neural trajectories along CD (Method details).

(B) Sessions with small (top row, $-0.2 <$ delta performance < 0.1) or big (bottom row, $-0.9 <$ delta performance < -0.6) performance change. Sessions were selected from tasks 1–5.

(C) Distributions of CD projections in sessions with small (top row) or large (bottom row) performance change. Orange denotes trials with contralateral inhibition (relative to the recording side). Difference of the distribution is quantified by d′ (Method details).

(D) Projections along CD in conditions with small (top row) or large (bottom row) performance change. The left schematic shows the small (top) or large (bottom) influence on the contralateral hemisphere during inhibition. Shading, SEM. Orange shading, delay inhibition.

(E) Influence on the contralateral hemisphere is correlated with behavioral performance change for individual sessions (n = 124). Influence on the contralateral hemisphere is quantified by the difference in the distribution along CD between control and inhibition trials (Method details). Triangle, lick-left trial; circle, lick-right trial. Filled, left ALM inhibition; unfilled, right ALM inhibition.

(F) Similar to (E), but data are grouped for individual mice (n = 28).

(G) Similar to (E), but data are grouped for different tasks (n = 5).

(H) Left, schematic to illustrate the relation between influence on the contralateral hemisphere and behavioral deficit. Right, summary of behavioral deficit and influence on the contralateral hemisphere across tasks (Method details). Tasks 1 and 3 (the left ALM dominance) are located in the third quadrant, and tasks 2 and 4 (the right ALM dominance) are located in the first quadrant. Thus, the more deviated from the center, the more asymmetry between the 2 hemispheres.

See also Figures S6 and S7.

sensorimotor experience, are implied to contribute to the formation of lateralized brain functions (Michel et al., 2016; Sun and Walsh, 2006). Consistent hand usage preference during infancy can predict advanced language skills in toddlers (Nelson et al., 2014). Different organization of neural circuits enables specialized functions that are preferentially localized in one hemisphere. Our finding, that the left and right ALM contribute to STM differently in tasks with different sensorimotor association, bears the same essence that one side of the hemisphere plays a dominant role. Although it is not clear to which degree our finding can be extended to understand the lateralization in humans, sensorimotor experience may be an important factor in the development of hemispheric difference.

Correlated activity does not necessarily contribute to behavior

Neural activity exhibits a similar response pattern and has a similar encoding power across hemispheres (Figure 3). In the premotor cortex of monkeys, motor planning activity also shows similar responses during an upcoming reach or grasp using either the contralateral or ipsilateral arm (Cisek et al., 2003; Michaels and Scherberger, 2018). In the motor cortex of monkeys, similar muscle-related activity is found present in either hemisphere (Ames and Churchland, 2019; Heming et al., 2019). These results suggest that similar information present in either hemisphere may be a general phenomenon during STM and movement in multiple species.

Similar neural dynamics across the left and right ALM may suggest that both hemispheres play a similar role in STM. However, inhibition of the dominant side disrupts selective information in the non-dominant side to induce a large behavioral deficit, but not vice versa (Figures 1, 5, and 6). This demonstrates that correlated activity, even in an area that is known to be critical under certain contingencies, can play a minimal role under different conditions. These results underscore the importance of using temporal-specific perturbation methods to probe the causal contribution of neural activity. Determining the functional role of one brain area requires perturbation under different sensory-motor contingencies or even under different tasks.

Limitations of the study

Multiple factors, including different behavioral strategies, may underlie the hemispheric dominance we observed in our study. We do not understand the underlying strategies that animals used in different tasks, and the strategy may be varied across trials, sessions, animals, and tasks. However, we find that the asymmetric interaction between the left and right hemispheres not only accounts for the hemispheric difference in behavioral deficits across tasks but also explains varied deficits across sessions and mice. Understanding the strategy variations can further help to understand how behavioral deficits are caused by optogenetic perturbations. In this study, we focused on ALM and used relatively low laser power (1.5 mW) for photoinhibition. Inhibition during STM does not affect orofacial movements, suggesting that the perturbation mainly affects STM. However, as ALM is adjacent to other premotor and motor areas (e.g., ~1.3 mm away from the tongue-jaw motor cortex), optogenetic perturbation may partially affect nearby regions.

STAR★METHODS

Detailed methods are provided in the online version of this paper and include the following:

- KEY RESOURCES TABLE
- RESOURCE AVAILABILITY
  - Lead contact
  - Materials availability
  - Data and code availability
- EXPERIMENTAL MODEL AND SUBJECT DETAILS
  - Mice
- METHOD DETAILS
  - Behavior
  - Surgery
  - Photoinhibition of ALM
  - Extracellular electrophysiology
  - Videography
- QUANTIFICATION AND STATISTICAL ANALYSIS
  - Behavioral data analysis
  - Electrophysiology data analysis
  - Hierarchical clustering
  - Population vector analysis
  - Decoding of choice
- NOISE CORRELATIONS
  - Statistics

SUPPLEMENTAL INFORMATION

Supplemental information can be found online at https://doi.org/10.1016/j.celrep.2022.111190.

ACKNOWLEDGMENTS

We thank Hidehiko Inagaki, Nuo Li, Zheng Wu, Jorge Jaramillo, Ning-long Xu, Kexin Yuan, and Susu Chen for comments on the manuscript, and the animal core facility at Tsinghua University for maintaining the mouse lines. This work was supported by the National Natural Science Foundation of China (32021002 and 32170998) to Z.V.G.

AUTHOR CONTRIBUTIONS

X.Y. performed the experiments, with input from Y.W. and J.L. (photoinhibition in five mice under the standard contingency). X.Y. analyzed the data. X.Y. and Z.V.G. conceived the project. X.Y. and Z.V.G. wrote the paper, with comments from the other authors.

DECLARATION OF INTERESTS

The authors declare no competing interests.

Received: October 26, 2021
Revised: June 4, 2022
Accepted: July 20, 2022
Published: August 16, 2022

REFERENCES

Aljundi, R., Chakravarty, P., and Tuytelaars, T. (2017). Expert gate: lifelong learning with a network of experts. In Paper presented at: Proceedings of the IEEE Conference on Computer Vision and Pattern Recognition.

Ames, K.C., and Churchland, M.M. (2019). Motor cortex signals for each arm are mixed across hemispheres and neurons yet partitioned within the population response. Elife *8*, e46159.

Baddeley, A.D., and Hitch, G. (1974). Working memory. Psychol. Learn. Motiv. *8*, 47–89.

Blumenfeld, H. (2002). Neuroanatomy through Clinical Cases (Sinauer associates).

Bogen, J.E., and Bogen, G.M. (1976). Wernicke's region–Where is it? Ann. N. Y. Acad. Sci. *280*, 834–843.

Borod, J.C., Andelman, F., Obler, L.K., Tweedy, J.R., and Welkowitz, J. (1992). Right hemisphere specialization for the identification of emotional words and sentences: evidence from stroke patients. Neuropsychologia *30*, 827–844.

Brincat, S.L., Donoghue, J.A., Mahnke, M.K., Kornblith, S., Lundqvist, M., and Miller, E.K. (2021). Interhemispheric transfer of working memories. Neuron *109*, 1055–1066.e4.

Chen, G., Kang, B., Lindsey, J., Druckmann, S., and Li, N. (2021). Modularity and robustness of frontal cortical networks. Cell *184*, 3717–3730.e24.

Chéreau, R., Bawa, T., Fodoulian, L., Carleton, A., Pagès, S., and Holtmaat, A. (2020). Dynamic perceptual feature selectivity in primary somatosensory cortex upon reversal learning. Nat. Commun. *11*, 3245.

Christophel, T.B., Klink, P.C., Spitzer, B., Roelfsema, P.R., and Haynes, J.D. (2017). The distributed nature of working memory. Trends Cogn. Sci. *21*, 111–124.

Cisek, P., Crammond, D.J., and Kalaska, J.F. (2003). Neural activity in primary motor and dorsal premotor cortex in reaching tasks with the contralateral versus ipsilateral arm. J. Neurophysiol. *89*, 922–942.

Cohen, M.R., and Kohn, A. (2011). Measuring and interpreting neuronal correlations. Nat. Neurosci. *14*, 811–819.

Corballis, M.C. (2003). From mouth to hand: gesture, speech, and the evolution of right-handedness. Behav. Brain Sci. *26*, 199–208. discussion 208-160.

Defelipe, J. (2011). The evolution of the brain, the human nature of cortical circuits, and intellectual creativity. Front. Neuroanat. *5*, 29.

Deisseroth, K. (2015). Optogenetics: 10 years of microbial opsins in neuroscience. Nat. Neurosci. *18*, 1213–1225.

Diamond, M.E., von Heimendahl, M., Knutsen, P.M., Kleinfeld, D., and Ahissar, E. (2008). 'Where' and 'what' in the whisker sensorimotor system. Nat. Rev. Neurosci. *9*, 601–612.

Dronkers, N.F., Plaisant, O., Iba-Zizen, M.T., and Cabanis, E.A. (2007). Paul Broca's historic cases: high resolution MR imaging of the brains of Leborgne and Lelong. Brain *130*, 1432–1441.

Ehret, G. (1987). Left hemisphere advantage in the mouse brain for recognizing ultrasonic communication calls. Nature *325*, 249–251.

Erlich, J.C., Bialek, M., and Brody, C.D. (2011). A cortical substrate for memory-guided orienting in the rat. Neuron *72*, 330–343.

Esmaeili, V., Tamura, K., Muscinelli, S.P., Modirshanechi, A., Boscaglia, M., Lee, A.B., Oryshchuk, A., Foustoukos, G., Liu, Y., Crochet, S., et al. (2021). Rapid suppression and sustained activation of distinct cortical regions for a delayed sensory-triggered motor response. Neuron *109*, 2183–2201.e9.

Finkelstein, A., Fontolan, L., Economo, M.N., Li, N., Romani, S., and Svoboda, K. (2021). Attractor dynamics gate cortical information flow during decision-making. Nat. Neurosci. *24*, 843–850.

Fridman, E.A., Hanakawa, T., Chung, M., Hummel, F., Leiguarda, R.C., and Cohen, L.G. (2004). Reorganization of the human ipsilesional premotor cortex after stroke. Brain *127*, 747–758.

Frost, S.B., Barbay, S., Friel, K.M., Plautz, E.J., and Nudo, R.J. (2003). Reorganization of remote cortical regions after ischemic brain injury: a potential substrate for stroke recovery. J. Neurophysiol. *89*, 3205–3214.

Funahashi, S., Bruce, C.J., and Goldman-Rakic, P.S. (1989). Mnemonic coding of visual space in the monkey's dorsolateral prefrontal cortex. J. Neurophysiol. *61*, 331–349.

Fuster, J.M., and Alexander, G.E. (1971). Neuron activity related to short-term memory. Science *173*, 652–654.

Gallero-Salas, Y., Han, S., Sych, Y., Voigt, F.F., Laurenczy, B., Gilad, A., and Helmchen, F. (2021). Sensory and behavioral components of neocortical signal flow in discrimination tasks with short-term memory. Neuron *109*, 135–148.e6.

Gao, Z., Davis, C., Thomas, A.M., Economo, M.N., Abrego, A.M., Svoboda, K., De Zeeuw, C.I., and Li, N. (2018). A cortico-cerebellar loop for motor planning. Nature *563*, 113–116.

Gazzaniga, M.S. (2000). Cerebral specialization and interhemispheric communication: does the corpus callosum enable the human condition? Brain *123*, 1293–1326.

Gilad, A., Gallero-Salas, Y., Groos, D., and Helmchen, F. (2018). Behavioral strategy determines frontal or posterior location of short-term memory in neocortex. Neuron *99*, 814–828.e7.

Goard, M.J., Pho, G.N., Woodson, J., and Sur, M. (2016). Distinct roles of visual, parietal, and frontal motor cortices in memory-guided sensorimotor decisions. Elife *5*, e13764.

Guo, Z.V., Hires, S.A., Li, N., O'Connor, D.H., Komiyama, T., Ophir, E., Huber, D., Bonardi, C., Morandell, K., Gutnisky, D., et al. (2014a). Procedures for behavioral experiments in head-fixed mice. PLoS One *9*, e88678.

Guo, Z.V., Inagaki, H.K., Daie, K., Druckmann, S., Gerfen, C.R., and Svoboda, K. (2017). Maintenance of persistent activity in a frontal thalamocortical loop. Nature *545*, 181–186.

Guo, Z.V., Li, N., Huber, D., Ophir, E., Gutnisky, D., Ting, J.T., Feng, G., and Svoboda, K. (2014b). Flow of cortical activity underlying a tactile decision in mice. Neuron *81*, 179–194.

Hanks, T.D., Kopec, C.D., Brunton, B.W., Duan, C.A., Erlich, J.C., and Brody, C.D. (2015). Distinct relationships of parietal and prefrontal cortices to evidence accumulation. Nature *520*, 220–223.

Hartwigsen, G., Bengio, Y., and Bzdok, D. (2021). How does hemispheric specialization contribute to human-defining cognition? Neuron *109*, 2075–2090.

Heilman, K.M., and Van Den Abell, T. (1980). Right hemisphere dominance for attention: the mechanism underlying hemispheric asymmetries of inattention (neglect). Neurology *30*, 327–330.

Heming, E.A., Cross, K.P., Takei, T., Cook, D.J., and Scott, S.H. (2019). Independent representations of ipsilateral and contralateral limbs in primary motor cortex. Elife *8*, e48190.

Hippenmeyer, S., Vrieseling, E., Sigrist, M., Portmann, T., Laengle, C., Ladle, D.R., and Arber, S. (2005). A developmental switch in the response of DRG neurons to ETS transcription factor signaling. PLoS Biol. *3*, e159.

Inagaki, H.K., Chen, S., Ridder, M.C., Sah, P., Li, N., Yang, Z., Hasanbegovic, H., Gao, Z., Gerfen, C.R., and Svoboda, K. (2022). A midbrain-thalamus-cortex circuit reorganizes cortical dynamics to initiate movement. Cell *185*, 1065–1081.e23.

Inagaki, H.K., Fontolan, L., Romani, S., and Svoboda, K. (2019). Discrete attractor dynamics underlies persistent activity in the frontal cortex. Nature *566*, 212–217.

Inagaki, H.K., Inagaki, M., Romani, S., and Svoboda, K. (2018). Low-dimensional and monotonic preparatory activity in mouse anterior lateral motor cortex. J. Neurosci. *38*, 4163–4185.

Jonides, J., Lewis, R.L., Nee, D.E., Lustig, C.A., Berman, M.G., and Moore, K.S. (2008). The mind and brain of short-term memory. Annu. Rev. Psychol. *59*, 193–224.

Jun, J.J., Mitelut, C., Lai, C., Gratiy, S.L., Anastasiades, C.A., and Harris, T.D. (2017). Real-time spike sorting platform for high-density extracellular probes with ground-truth validation and drift correction. Preprint at bioRxiv.

Klur, S., Muller, C., Pereira de Vasconcelos, A., Ballard, T., Lopez, J., Galani, R., Certa, U., and Cassel, J.C. (2009). Hippocampal-dependent spatial memory functions might be lateralized in rats: an approach combining gene expression profiling and reversible inactivation. Hippocampus *19*, 800–816.

Kopec, C.D., Erlich, J.C., Brunton, B.W., Deisseroth, K., and Brody, C.D. (2015). Cortical and subcortical contributions to short-term memory for orienting movements. Neuron *88*, 367–377.

Li, N., Chen, S., Guo, Z.V., Chen, H., Huo, Y., Inagaki, H.K., Chen, G., Davis, C., Hansel, D., Guo, C., and Svoboda, K. (2019). Spatiotemporal constraints of optogenetic inactivation in cortical circuits. Elife *8*, e48622.

Li, N., Chen, T.W., Guo, Z.V., Gerfen, C.R., and Svoboda, K. (2015). A motor cortex circuit for motor planning and movement. Nature *519*, 51–56.

Li, N., Daie, K., Svoboda, K., and Druckmann, S. (2016). Robust neuronal dynamics in premotor cortex during motor planning. Nature *532*, 459–464.

Liu, Y., and Rouiller, E.M. (1999). Mechanisms of recovery of dexterity following unilateral lesion of the sensorimotor cortex in adult monkeys. Exp. Brain Res. *128*, 149–159.

Luo, L., Callaway, E.M., and Svoboda, K. (2018). Genetic dissection of neural circuits: a decade of progress. Neuron *98*, 865–881.

Marlin, B.J., Mitre, M., D'amour, J.A., Chao, M.V., and Froemke, R.C. (2015). Oxytocin enables maternal behaviour by balancing cortical inhibition. Nature *520*, 499–504.

Mayrhofer, J.M., El-Boustani, S., Foustoukos, G., Auffret, M., Tamura, K., and Petersen, C.C.H. (2019). Distinct contributions of whisker sensory cortex and tongue-jaw motor cortex in a goal-directed sensorimotor transformation. Neuron *103*, 1034–1043.e5.

Michaels, J.A., and Scherberger, H. (2018). Population coding of grasp and laterality-related information in the macaque fronto-parietal network. Sci. Rep. *8*, 1710.

Michel, G.F., Campbell, J.M., Marcinowski, E.C., Nelson, E.L., and Babik, I. (2016). Infant hand preference and the development of cognitive abilities. Front. Psychol. *7*, 410.

Musall, S., Kaufman, M.T., Juavinett, A.L., Gluf, S., and Churchland, A.K. (2019). Single-trial neural dynamics are dominated by richly varied movements. Nat. Neurosci. *22*, 1677–1686.

Nelson, E.L., Campbell, J.M., and Michel, G.F. (2014). Early handedness in infancy predicts language ability in toddlers. Dev. Psychol. *50*, 809–814.

Nielsen, J.A., Zielinski, B.A., Ferguson, M.A., Lainhart, J.E., and Anderson, J.S. (2013). An evaluation of the left-brain vs. right-brain hypothesis with resting state functional connectivity magnetic resonance imaging. PLoS One *8*, e71275.

Pho, G.N., Goard, M.J., Woodson, J., Crawford, B., and Sur, M. (2018). Task-dependent representations of stimulus and choice in mouse parietal cortex. Nat. Commun. *9*, 2596.

Pool, E.M., Rehme, A.K., Fink, G.R., Eickhoff, S.B., and Grefkes, C. (2014). Handedness and effective connectivity of the motor system. Neuroimage *99*, 451–460.

Price, C.J. (2010). The anatomy of language: a review of 100 fMRI studies published in 2009. Ann. N. Y. Acad. Sci. *1191*, 62–88.

Rogers, L.J., Zucca, P., and Vallortigara, G. (2004). Advantages of having a lateralized brain. Proc. Biol. Sci. *271*, S420–S422.

Romo, R., Brody, C.D., Hernández, A., and Lemus, L. (1999). Neuronal correlates of parametric working memory in the prefrontal cortex. Nature *399*, 470–473.

Roy, N.A., Bak, J.H., International Brain Laboratory; Akrami, A., Brody, C.D., and Pillow, J.W. (2021). Extracting the dynamics of behavior in sensory decision-making experiments. Neuron *109*, 597–610.e6.

Rusu, A.A., Rabinowitz, N.C., Desjardins, G., Soyer, H., Kirkpatrick, J., Kavukcuoglu, k., Pascanu, R., and Hadsell, R. (2016). Progressive neural networks. Preprint at arXiv. https://doi.org/10.48550/arXiv.1606.04671.

Siegle, J.H., López, A.C., Patel, Y.A., Abramov, K., Ohayon, S., and Voigts, J. (2017). Open Ephys: an open-source, plugin-based platform for multichannel electrophysiology. J. Neural. Eng. *14*, 045003.

Sperry, R.W. (1968). Hemisphere deconnection and unity in conscious awareness. Am. Psychol. *23*, 723–733.

Sperry, R.W., Gazzaniga, M.S., and J.E., B. (1969). Interhemispheric relationships: the neocortical commissures; syndromes of hemisphere disconnection. In Handb. Clin. Neurol., *No.4* (North-Holland Publishing Co.), pp. 273–290.

Stringer, C., Pachitariu, M., Steinmetz, N., Reddy, C.B., Carandini, M., and Harris, K.D. (2019). Spontaneous behaviors drive multidimensional, brainwide activity. Science *364*, 255.

Sun, T., and Walsh, C.A. (2006). Molecular approaches to brain asymmetry and handedness. Nat. Rev. Neurosci. *7*, 655–662.

Svoboda, K., and Li, N. (2018). Neural mechanisms of movement planning: motor cortex and beyond. Curr. Opin. Neurobiol. *49*, 33–41.

Tanji, J., and Evarts, E.V. (1976). Anticipatory activity of motor cortex neurons in relation to direction of an intended movement. J. Neurophysiol. *39*, 1062–1068.

Vallortigara, G. (2006). The evolutionary psychology of left and right: costs and benefits of lateralization. Dev. Psychobiol. *48*, 418–427.

Vallortigara, G., and Rogers, L.J. (2005). Survival with an asymmetrical brain: advantages and disadvantages of cerebral lateralization. Behav. Brain Sci. *28*, 575–589. discussion 589-633.

Wang, Y., Yin, X., Zhang, Z., Li, J., Zhao, W., and Guo, Z.V. (2021). A cortico-basal ganglia-thalamo-cortical channel underlying short-term memory. Neuron *109*, 3486–3499.e7.

Witelson, S.F., and Pallie, W. (1973). Left hemisphere specialization for language in the newborn. Neuroanatomical evidence of asymmetry. Brain *96*, 641–646.

Wu, Z., Litwin-Kumar, A., Shamash, P., Taylor, A., Axel, R., and Shadlen, M.N. (2020). Context-dependent decision making in a premotor circuit. Neuron *106*, 316–328.e6.

STAR★METHODS

KEY RESOURCES TABLE

REAGENT or RESOURCE	SOURCE	IDENTIFIER
Experimental models: Organisms/strains		
Mouse: Rosa26 CAG-LSL-ReaChR-mCit	The Jackson Laboratory	Stock No. 026294
Mouse: PV-Cre	The Jackson Laboratory	Stock No. 008069
Software and algorithms		
MATLAB 2017b & 2019a	MathWorks	https://www.mathworks.com/products/matlab.html; RRID: SCR_001622
Python3.8; Anaconda distribution	https://anaconda.com	N/A
LabVIEW	National Instruments	http://www.ni.com/enus/shop/labview.html; RRID: SCR_014325
SpikeGLX	Janelia Research Campus	https://billkarsh.github.io/SpikeGLX
Kilosort2	Stringer et al., 2019	https://www.github.com/MouseLand/Kilosort2
JRCLUST	Jun et al., 2017	https://github.com/JaneliaSciComp/JRCLUST
FlyCapture	FLIR	N/A
Other		
594 nm laser	Obis LS, Coherent Chang Chun Optics	OBIS 594–100 mW MGL-N-593.5 nm-200 mW
Acousto-optical modulato	Quanta Tech	MTS110-A3-VIS
64-channel silicon probes	Cambridge NeuroTech	ACUTE-64-4–250 probe
NeuroPixels probes	Imec	NeuroPixels 1.0
Scanning galvo	Thorlabs	GVS012
CMOS camera	FLIR	CM3-U3-13Y3M
Deposited data	This paper; Mendeley Data	https://doi.org/10.17632/vpwsttrjfh.1

RESOURCE AVAILABILITY

Lead contact

Further information and requests for resources and reagents should be directed to and will be fulfilled by the lead contact, Zengcai V. Guo (guozengcai@tsinghua.edu.cn).

Materials availability

This study did not generate new unique reagents.

Data and code availability

- The behavior and electrophysiology data generated during this study are available at Mendeley Data (https://doi.org/10.17632/vpwsttrjfh.1).
- The MATLAB and Python code used to produce main results of this study are available at Mendeley Data (https://doi.org/10.17632/vpwsttrjfh.1).
- Any additional information required to reanalyze the data reported in this paper is available from the lead contact upon request.

EXPERIMENTAL MODEL AND SUBJECT DETAILS

Mice

This study is based on data from 84 PV-IRES-Cre (JAX 008069) (Hippenmeyer et al., 2005) × R26-CAG-LSL-ReaChR-mCitrine (JAX 026294) (Li et al., 2019) transgenic mice (shorted as PV-ReaChR). There were 32, 22, 9, 7 and 14 mice trained in tasks 1–5 respectively (age > P60, male). All experimental procedures were approved by the Institutional Animal Care and Use Committee at Tsinghua University, Beijing, China. Mice were housed with siblings to allow social interaction. A 12:12 reverse light: dark cycle was used and behavioral tests were done during the dark phase.

METHOD DETAILS

Behavior

The behavior training was modified from before (Guo et al., 2014a). A metal pole, attached to the shaft of a mirror galvanometer (with the attached mirror removed, Jinhaichuang Inc), was presented near the right side of whiskers of mice (~6 mm away from the base of whiskers). A two-spout lickport was used to record licking events and deliver milk as reward. During each trial, the pole was controlled by the galvanometer to vibrate with a sinusoidal profile at 10Hz, a frequency close to the frequency of natural whisking. The strength of the stimulus was adjusted by changing the current input to the galvanometer (1838°/s peak velocity for the strong stimulus and 408°/s peak velocity for the weak stimulus). For the standard contingency (task1), mice were trained to lick right for the strong stimulus and lick left for the weak stimulus in order to obtain a reward. For the reversed contingency (task2), the association between the stimulus and the licking side was reversed. The association between the stimulus and the licking side was the same between task 1 (task 2) and task 3 (task 4) except that simultaneous bilateral stimulation applied using two galvanometers in tasks 3 and 4. In task 5, mice were trained to associate the stimulation of the left (right) side of whiskers with licking the left (right) water spout. During training, the length of the delay epoch gradually increased from 0 s to 1 s. For the full task, the stimulus lasted for 1 s in the sample epoch which was followed by the delay epoch (1 s). Then an auditory go cue (0.1 s) signaled mice to response within a 1 s window. Correct licking during the response epoch resulted in a reward (~4μL milk). Licking during the sample or delay epoch (early-lick trials) would cause a timeout (1 s). Licking the incorrect lickport (error trials) or not licking within 1 s after the go cue (no response trials) would lead to no reward. These early-lick and no response trials were excluded from analyses of performance and neural activity.

Each behavioral session lasted for 56 ± 15 min with 374 ± 95 trials (mean ± standard deviation). After each training session, the mouse was supplied with additional 1.5–3 g food pellet (depending on the performance of the mouse on that day) to maintain a stable body weight (>85% of the weight before training).

Surgery

All surgical procedures were carried out aseptically under 1.5–2% isoflurane anesthesia. Flunixin meglumine (Sichuan Dingjian Animal Medicine Co., Ltd) was injected subcutaneously (1.25 mg/kg) during and after the surgery for at least three days to reduce inflammation.

Mice were prepared for electrophysiology and photostimulation with a head bar and a clear-skull cap (Guo et al., 2014b). The scalp of the mouse was removed to expose the skull covering the dorsal cortex. After clearing the exposed cranium, a thin layer of cyanoacrylate adhesive (Krazy glue, Elmer's Products Inc) was directly applied to the intact skull. A custom titanium bar was glued to the skull (approximately over the cerebellum). Two holes were drilled over the cerebellum and two silver pins (made by soldering a thin wire to a metal pin, Digi-Key Part Number, ED90488-ND) were inserted into the holes as the ground and reference pins during electrophysiology. Dental acrylic (Lang Dental Jet Repair Acrylic; Part# 1223-clear) was applied to cement the head bar in place. To increase light delivery efficiency through the skull, the dental acrylic was polished and covered by a thin layer of clear nail polish (Electron Microscopy Sciences, Part# 72,180).

For extracellular recording in ALM, a small craniotomy (~2 mm^2 square) was made one day before the recording, to allow the electrode to penetrate through the dura. After craniotomy or recording, the exposed brain was covered by artificial dura and silica gel for protection (Guo et al., 2014b).

Photoinhibition of ALM

PV-ReaChR transgenic mice were used for ALM photoinhibition (laser spot focused at bregma +2.5, lateral 1.5 mm). Inhibition by activating parvalbumin (PV) interneurons achieved similar inhibition effects with stimulating GABAergic neurons in VGAT-ChR2-EYFP mice (Li et al., 2019). Photoinhibition was deployed randomly on 25% of trials. To prevent mice from distinguishing photoinhibition trials from control trials by visual cues, an LED pulse train was delivered near the eyes of the mice (i.e. 'masking flash', 40 × 1ms pulses at 10 Hz, Luxeon Star). The masking flash began 1s before the start of a trial and ended when the trial finished.

Orange light from a 594 nm laser (Obis LS, Coherent or Chang Chun optics) was controlled by an acoustic-optic modulator (AOM; MTS110-A3-VIS, Quanta Tech; extinction ratio 1:2000). A mechanical shutter (Uniblitz LS6S2T0, Vincent Associates) was used to block light completely for non-photoinhibition periods. A 2D scanning galvo system (GVS012, Thorlabs) was used to deliver light to the left ALM or right ALM (AP 2.5, ML ±1.5 mm) through the clear-skull cap implant. The light transmission efficiency through the intact skull is ~50% (Guo et al., 2014b).

For unilateral inhibition, a laser with 40-Hz sinusoidal temporal profile (mean laser power, 1.5 mW) was randomly directed to the left or right ALM during the sample or delay epoch. The clear skull preparation had a light transmission efficiency about 50% (Guo et al., 2014b). The protocol could achieve robust inhibition with ~90% of spikes silenced in a cortical area of a 1 mm radius (at half-max) through all cortical layers (Li et al., 2019). The laser power was linearly ramped down for 100 ms to minimize the rebound excitation after photoinhibition (Guo et al., 2014b).

Extracellular electrophysiology

All recordings were made from the left or right ALM from head-fixed behaving mice. Extracellular spikes were recorded by 64-channel silicon probes (4 shank probes with 250 μm shank spacing and 25 μm site spacing, P-series, Cambridge NeuroTech) or 32-channel

silicon probes (4 shank probes with 200 μm shank spacing and 100 μm linear site spacing, P/N A4x8-5mm-100-200–177, NeuroNexus). The voltage signals were acquired by the OpenEphys acquisition system (each channel sampled at 25 kHz, http://www.open-ephys.org) (Siegle et al., 2017). For simultaneous bilateral recordings, we advanced two NeuroPixels probes (NeuroPixels 1.0) in the left and right ALM. The voltage signals were acquired through SpikeGLX.

There were typically 2–4 penetrations through each craniotomy. For 64-channel silicon probes with recording sites covering only ~200μm in depth, there were typically ~2 recording sessions in one penetration. Between sessions (lasting for ~10 min), the probe was driven at least 200 um deeper by a micromanipulator (Sutter Instrument). The tissue was allowed to settle for at least 5 min before the recording started. During electrophysiology, the contralateral ALM was randomly inhibited in 25 or 33% of trials during the sample or delay epochs. The inhibition protocol was the same as the one spot inhibition (40-Hz sinusoidal temporal profile, mean laser power 1.5 mW, 100 ms linear ramping down). For recordings using NeuroPixels probes, the recording sites covered layers 1–6 as the shank with recording sites spanning about 10mm.

Videography

Orofacial movements were captured by two cameras (CM3-U3-13Y3M, FLIR) from the bottom and side of the animal head. Mice were illuminated with infrared light (850 nm). The focal length of the equipped camera lens is 16mm (FA1601C, Chiopt). A filter (BP850, AZURE) with infrared bandpass was used to block visible light including the orange light used in optogenetic inhibition experiments. The frame rate of the camera was set to 203Hz with 1ms exposure time. We manually selected 3 regions of interest (ROI) to represent the movement of jaw, whisker pad and nose (results were not sensitive to exact positions, Figure S7). The motion energy for each ROI was computed as the absolute difference between two consecutive images (Mayrhofer et al., 2019; Musall et al., 2019; Stringer et al., 2019). To quantify the motion during unilateral or bilateral inhibition, inhibition trials were randomly interleaved with 25% probability. Bilateral inhibition was achieved by alternatively directing the laser spot, using a galvo mirror, to the left and right ALMs. The alternating frequency is 200Hz and each ALM was illuminated for 5ms (including traveling time). The laser power was adjusted according to the number of spots to reach an average power of 1.5mW. Trials with mean motion energy during the delay epoch lower than a threshold were defined as quiet trials. The threshold was calculated as the pre-sample (1s) mean motion energy minus 0.8 times standard deviation. These quiet trials with little movement in jaw, whisker pad and nose accounted for 3.9%, 9.7% and 1.4% of all trials, respectively.

QUANTIFICATION AND STATISTICAL ANALYSIS

Behavioral data analysis

Behavior performance was calculated as the fraction of correct trials, excluding 'lick early' and 'no response' trials. 'Lick early' rate was the fraction of trials in which mice licked before the response epoch. 'No response rate' was the fraction of trials in which mice did not lick during the response period. We separately computed the performance for left and right trials. Behavioral effects of photoinhibition were quantified by comparing the performance during photoinhibition with control performance. To compare the inhibition effects between the left and right ALM during the delay epoch, we defined the 'combined deficit', which was the summation of ipsilateral bias in lick-left and lick-right trials (i.e. performance increase in lick-left trials minus performance decrease in lick-right trials for photoinhibition of the left ALM; performance increase in lick-right trials minus performance decrease in lick-left trials for the right ALM). The significance of change in performance was determined using two-sided Student's *t*-test. To compare the difference of combined deficit due to the inhibition of the left or right ALM, we used bootstrap to determine the significance (10,000 random sampling across different sessions). PsyTrack was used to measure possible bias and dependence on history (Roy et al., 2021). Early and late training sessions were concatenated and fed into PsyTrack with default parameters.

Electrophysiology data analysis

For recordings using 64-channel or 32-channel silicon probes, the extracellular traces were band-filtered (300–6000 Hz). Events that exceeded an amplitude threshold (4 standard deviations of the background) were sorted using JRclust (Jun et al., 2017). For recordings using NeuroPixels probes, we used Kilosort2 to perform clustering (Stringer et al., 2019). Before feeding the data into Kilosort2, we first used CatGT (https://billkarsh.github.io/SpikeGLX/) to subtract the averaged value of the signals sampled at the same time to reduce the common noise. Kilosort2 could give many candidate clusters (even up to thousands). We used the pipeline developed by the Allen Institute for Brain Science (ephys_spike_sorting) to select high quality units: 1) removing repeated spikes in each cluster, 2) finding clusters that were likely to be noise, 3) calculating the properties of each cluster and 4) using the quality matrix to select units. Selected units need to meet the following criteria: 1) they were annotated by Kilosort2 as 'Single Unit'. 2) they were not annotated as a noise cluster, 3) the average firing rate was higher than 1 Hz, 4) the average amplitude of the waveform was higher than 100 μV, 5) the estimated time of appearance was higher than 0.8.

For recordings using 64-channel or 32-channel silicon probes, we isolated 3393 single-units from ALM across 97 behavior sessions in 16 mice. Units were distributed across layers but a large portion were recorded from layer 5 because units there typically had higher firing rates and the recording in deeper layers seemed to be more stable (Figure S1F). Spike width was calculated as the trough-to-peak interval in the mean spike waveform. The distribution of spike widths was bimodal (Figure S1); units with width <0.4 ms were defined as putative fast-spiking (FS) neurons (298/3393) and units with width >0.6 ms as putative pyramidal neurons

(PPy neurons, 2423/3393). The classification was previously verified by optogenetic tagging of GABAergic neurons (Guo et al., 2014b). For recordings using NeuroPixels probes, we isolated 5796 single-units from 71 behavior sessions in 20 mice. Spikes recorded by NeuroPixels probes were high-pass filtered, which would reduce the spike width. So neurons with a width <0.3 were regarded as FS (1007/5796). Neurons with a width >0.3 and <0.6 were regarded as PPy (4789/4936). This classification criterion was verified in Figure S4E. We focused our analyses on putative pyramidal neurons, though the main results were similar when all neurons were included.

For task 1, we collected 1232/1678 PPy neurons in the left ALM across 42 behavior sessions in 9 mice. In the right ALM, we isolated 1373/1755 PPy neurons across 44 behavior sessions in 11 mice. To quantify the relationship between orofacial movements and neural activities in ALM, we further recorded 372/447 in the left ALM and 350/413 PPy neurons in the right ALM (n = 4 mice, 11 sessions; Figure S7). For task 2, we isolated 658/900 PPy neurons in the left ALM (n = 7 mice, 29 sessions) and 722/961 PPy neurons in the right ALM (n = 7 mice, 28 sessions). For task 3, we isolated 284/345 PPy neurons in the left ALM (n = 4 mice, 13 sessions) and 507/609 PPy neurons in the right ALM (n = 4 mice, 13 sessions). For task 4, we isolated 300/356 PPy neurons in the left ALM (n = 4 mice, 13 sessions) and 438/513 PPy neurons in the right ALM (n = 4 mice, 14 sessions). For task 5, we isolated 409/513 PPy neurons in the left ALM (n = 4 mice, 14 sessions) and 567/699 PPy neurons in the right ALM (n = 4 mice, 14 sessions). Neurons were tested for trial type differentiation capability during the sample, delay, or response epoch by comparing spike counts during lick-left and lick-right trials (*Mann-Whitney U* test, $p < 0.01$). Neurons that significantly differentiated trial-types during any one of the trial epochs were deemed as "selective" (4875/6490, 75.1% for PPy neurons; 816/1167, 69.9% for FS neurons). Neurons selective during the sample or delay epoch were classified as having "preparatory activity". Neurons selective during the response epoch were classified as having "peri-movement selectivity". Neurons selective during any of the three epochs were further classified into 'left-preferring neurons' if the total spike counts during that epoch was higher in lick-left trials (or 'right-preferring neurons' if the total spike counts during that epoch was higher in lick-right trials). Only correct trials were included to classify neurons.

Selectivity for each neuron was computed as the firing rate difference between the preferred trials and non-preferred trials (Figure 3B). Selectivity with 1 ms bin was smoothed using a 200 ms window. Bootstrapping was used to estimate the standard errors of the mean selectivity.

For the peri-stimulus time histograms (PSTHs), correct and incorrect trials were included if not otherwise specified as photoinhibition changed neural activity irrespective of the response outcomes. Spikes were averaged using a 100 ms window. Bootstrapping was used to estimate standard errors of the mean.

To compute the mean firing rate of a neuron, spikes in contra- and ipsi-trials were combined (correct and incorrect trials, units with at least 6 perturbation trials). The Student's *t*-test was used to determine whether the neuron significantly changed its mean firing rate during perturbation relative to the control without perturbation ($p < 0.05$). To compare whether the portion of significantly modulated neurons was different across the two hemispheres, we used the chi-squared test to determine the significance (Figure S5C).

Hierarchical clustering

To categorize the response types of neuronal activities in the left and right ALM, we performed hierarchical clustering based on MATLAB function pdist, linkage and cluster. The mean PSTH of each trial types (correct lick-left trials and correct lick-right trials) were concatenated for each neuron, and neurons in the left ALM and right ALM for each task were combined during clustering. We set the procedure to first give 150 candidate clusters. We then computed the pairwise correlations of mean PSTH of these clusters, and clusters with correlations higher than 0.75 were combined. The process was stopped until no pairwise correlations were higher than 0.75. Only the sample and delay epochs (0–2 s) were included for clustering. In figure S3, only clusters accounting for more than 1% of all neurons were shown. Bootstrap was used to determine the significance when comparing the difference about the fraction of each cluster in the left and right ALM.

Population vector analysis

The coding direction (CD) is an n-dimensional vector in neural activity space that maximally distinguish lick-left and lick-right trials (Li et al., 2016). For simultaneously recorded n neurons, we calculated the spike rates in lick-left and lick-right trials separately for each neuron. Then, we obtained n-dimensional vectors $\overrightarrow{SR}_{t,right}$ and $\overrightarrow{SR}_{t,left}$ at each time point t (the dimension is n*1). The difference of the mean firing rate between lick-right and lick-left trials was defined as $\overrightarrow{w}_t = \overrightarrow{SR}_{t,right} - \overrightarrow{SR}_{t,left}$. The coding direction $\overrightarrow{CD}_t$ was then calculated by dividing the $\overrightarrow{w}_t$ by its own norm. For each session, we randomly selected half of trials to compute CD and projected the remaining half of trials to the CD to obtain trajectories. Sessions with at least 10 simultaneously recorded neurons and at least 10 trials for each trial type during control and perturbation conditions were selected. The neural trajectories were smoothed with a 200 ms time window (10 ms step). Because the CD is stable during the late delay period (data not shown) (Li et al., 2016), we averaged CD during the last 500ms of the delay epoch. The CD could explain a large portion of the averaged selectivity (70.3%, data not shown) (Li et al., 2016).

To decode the choice based on trajectories along the CD, we defined the discrimination boundary (DB) that could maximally separate the left and right trajectories ($Traj_l$ and $Traj_r$, averaged on the last 500 ms during the delay epoch for each trial).

$$DB = \frac{\frac{mean(Traj_l)}{\sigma_l^2} + \frac{mean(Traj_r)}{\sigma_r^2}}{\frac{1}{\sigma_l^2} + \frac{1}{\sigma_r^2}}$$

mean($Traj$) represents averaged trajectory across left and right trials. σ^2 denotes the variance. For each session, we randomly selected half of correct trials to calculate DB and used the remaining trials to decode the performance. Sessions with at least 10 simultaneously recorded neurons were included.

After being projected along CD, trajectory endings in each trial type formed a distribution (Figure 7B). Unilateral inhibition of ALM in different tasks variably shifted the distribution in the contralateral hemisphere. To quantify the distance between the distribution during unilateral inhibition and during control, we calculated the d prime:

$$d' = \frac{|mean(I) - mean(C)|}{\sqrt{\frac{var(I) + var(C)}{2}}}$$

I and C represent the distribution of CD projections (relative to the decision boundary) during unilateral inhibition and during control, respectively. *mean* and *var* represent the average and the variance of the distribution, respectively. To quantify the degree of unilateral inhibition on contralateral activity, we defined the influence on the contralateral hemisphere (ICH) as:

$$\text{Influence on contralateral hemisphere (ICH)} = \frac{|mean(I)| - |mean(C)|}{\sqrt{\frac{var(I) + var(C)}{2}}}$$

To calculate ICH, the lick-left and lick-right trials were used separately (Figures 7E–7G). To quantify the overall effect about the ICH, we combined the lick-left and lick-right trials in Figure 7H. Similar to the combined deficit, ICH was the summation of ipsilateral bias in lick-left and lick-right trials (i.e. ICH increase in lick-left trials minus ICH decrease in lick-right trials for photoinhibition of the left ALM; ICH increase in lick-right trials minus ICH decrease in lick-left trials for the right ALM).

Decoding of choice

The procedure to decode choice was the same as that in our previous work (Wang et al., 2021). To quantify the coding capability of choice information of individual neurons, we first randomly selected n trials from each of the 4 trial types (lick-left correct, lick-left error, lick-right correct and lick-right error trials, n = 10 for each trial type, neurons with less than 10 trials for each trial type were not selected). We then calculated firing rates during the delay epoch for each selected trial. The coding of choice information was determined by comparing firing rates between trials that mice licked left and trials that mice licked right (firing rates in n lick-left correct trials and n lick-right error trials vs firing rates in n lick-left error trials and n lick-right correct trials). To quantify the difference between firing rates in selected groups of trials, we first drew the receiver operating characteristic curve (ROC), and then calculated the area under the curve (AUC). If AUC was 0.5, it meant the fraction of false positive and false negative predictions were the same and thus the neuron did not encode choice information. If AUC was close to 1, the neuron discriminated trials nearly perfectly. If AUC was less than 0.5, we would subtract its value from 1 to get the final AUC. To get the standard deviation of AUC, we repeated the above steps 200 times. We then averaged AUC values to obtain the coding capability of choice information for each neuron.

To quantify the coding capability of selected population of neurons, we trained a support vector machine (SVM) classifier (fitcecoc function in MATLAB from Mathworks). Because the number of simultaneously recorded neurons were limited in a session, we constructed a pseudo-population for the SVM classifier in the following steps. 1) Neurons from different recording sessions were pooled together. 2) A set of n neurons were randomly selected (the number of neurons was variable to obtain a relationship between decoding accuracy and number of neurons). 3) A set of m trials were randomly selected from each of the 4 trial types (lick-left correct, lick-left error, lick-right correct and lick-right error trials, m = 10 for each trial type, neurons with less than 10 trials for each trial type were not selected). 4) The firing rate of each selected neuron was calculated for each trial type to form an n x 4m matrix. 5) An SVM algorithm was trained to classify different trials types (lick-left vs lick-right choice for decision information; lick-left vs lick-right trials for sensory information). The classification accuracy was obtained through m-fold cross-validation. That is, the data was evenly divided into m parts, and the model was trained with m-1 parts, and then the remaining part was used as testing dataset. This process was repeated m times to obtain the averaged classification accuracy. 6) To get the corresponding standard deviation, steps 2–5 were repeated 200 times. 7) To quantify the decoding accuracy as a function of the number of neurons, the number of selected neurons was varied between 1 and 500 and steps 2–6 were repeated to get the decoding accuracy for each value of n. Since n = 200 yielded good prediction, we used this fixed number of neurons to quantify the decoding accuracy at different time points along trial progression (step size, 50 ms; smoothing window, 100 ms; Figure 3F). To compare the encoding capability of neurons in the left and right hemispheres, we used the null hypothesis that there were no difference between neurons in the left and right ALM. Bootstrapped data (obtained from repeating steps 2–5) were used to estimate the p value to invalidate the null hypothesis. To compare the decoding accuracy of choice at different numbers of neurons (n = 1 to 300–500), we repeated steps 2–5 20 times as there were hundreds of n and the results with increased number of repetitions were similar (Figure 3E). For choice decoding, the accuracy increased with time during the delay epoch and we used the mean value for comparison (Figure 3F).

NOISE CORRELATIONS

To obtain noise correlation of a pair of simultaneously recorded neurons, we first subtracted mean activity from their trial-to-trial activity and calculated the Pearson correlation.

$$NC_{ij} = \frac{cov(u_i, u_j)}{\sqrt{var(u_i) * var(u_j)}}$$

u_i and u_j represents the activity of the i-th and j-th neuron, respectively. Activity in lick-left and lick-right trials were concatenated to form a one-dimensional vector (including the sample and delay epochs with bin size 100 ms). We tested that a smaller bin size of 50 ms yielded similar results. $cov(u_i, u_j)$ represents the covariance of u_i and u_j. For control, we shuffled the labels of these trials before concatenating them to form the one-dimensional vector. Signal correlation was the Pearson correlation of the mean activity of these neurons. To compare the noise correlation between different groups of neurons, we used bootstrap to account for variability in different animals, sessions and trials.

Statistics

We sorted 9189 single-units from the left and right ALM (including units recorded during videography). The sample sizes are larger than typically used size in the field (typically several hundred units per brain region). No statistical methods were used to determine the sample size. We did not exclude any animals for data analysis. Control and photoinhibition trials were randomly interleaved in a computer program. During spike sorting, experimenters cannot tell the trial type, so experimenters were blind to conditions. All comparisons using bootstrap are two-sided. See the above sessions on data analysis for details of statistics.

Cell Reports, Volume *40*

Supplemental information

Lateralization of short-term memory in the frontal cortex

Xinxin Yin, Yu Wang, Jiejue Li, and Zengcai V. Guo

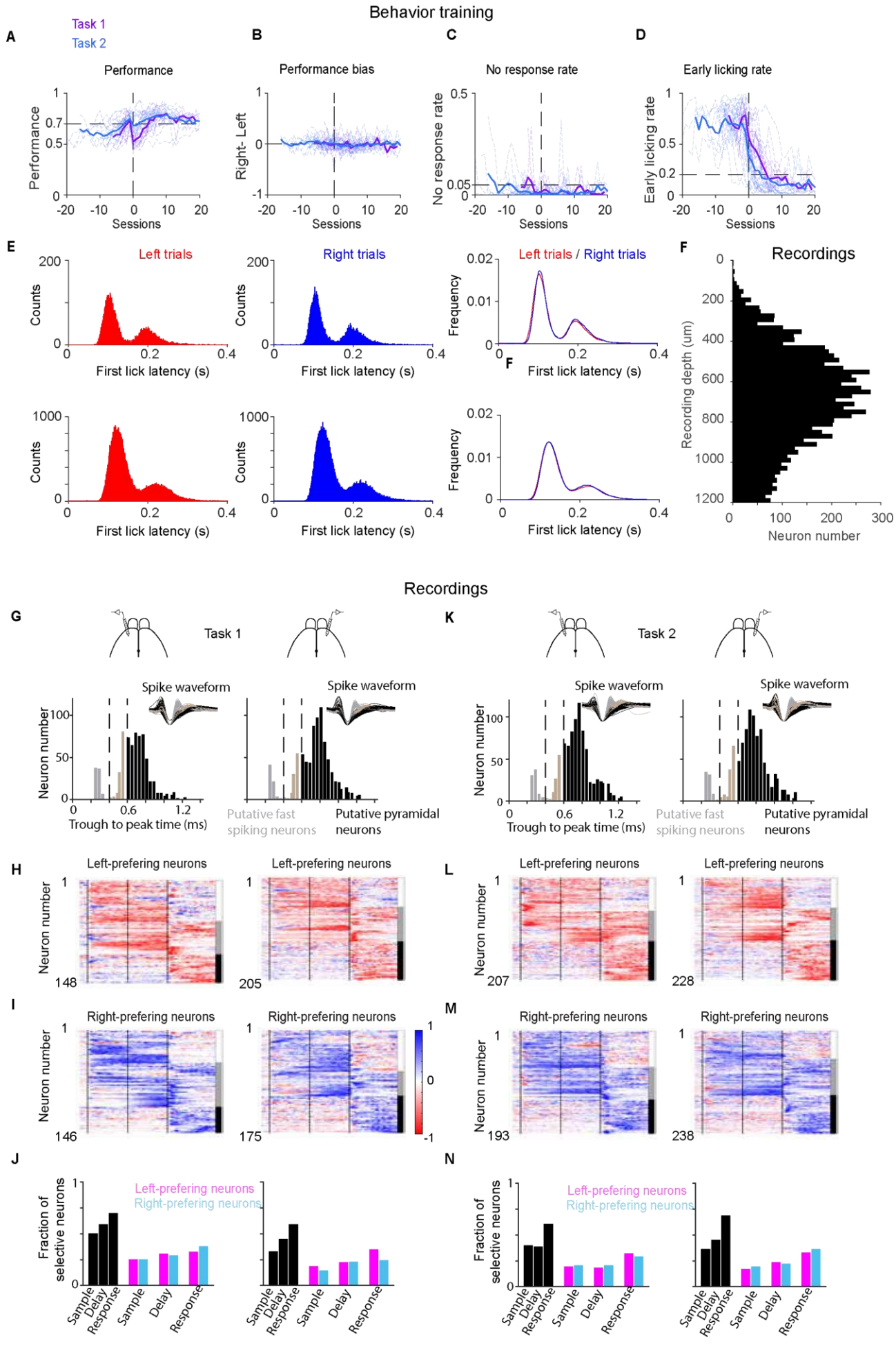
Behavior training
A
Task 1
Task 2
Performance
Performance
Sessions
B
Performance bias
Right- Left
Sessions
C
No response rate
No response rate
Sessions
D
Early licking rate
Early licking rate
Sessions
E
Left trials
Right trials
Left trials / Right trials
Counts
Frequency
First lick latency (s)
F
Recordings
Recording depth (um)
Neuron number
Recordings
G
Task 1
Spike waveform
Neuron number
Trough to peak time (ms)
Putative fast spiking neurons
Putative pyramidal neurons
K
Task 2
H
Left-prefering neurons
Neuron number
148
205
L
207
228
I
Right-prefering neurons
146
175
M
193
238
J
Fraction of selective neurons
Left-prefering neurons
Right-prefering neurons
Sample
Delay
Response
N

Figure S1. Behavioral training and recording under the standard and reversed contingencies, Related to Figure 1.

A. Learning curves. Sessions are aligned to the final step of training (i.e. adding the delay epoch). Thin lines, individual mice (standard contingency, n=11 mice; reversed contingency, n=22); thick lines, mean performance (for sessions with at least 4 mice). Only mice trained in the same training rig were included. Mice performed well, reaching a low 'no response rate' and no 'early licking rate' (performance, 83.7 ±0.5%; no response rate <0.05, early licking rate <0.2; **C**, **D**).

B. Performance bias between lick-right and lick-left trials. Same mice as in **A**. There was no bias for lick-left or lick-right trials during the training under either contingency (p>0.5, t-test).

C. No response rate. Same mice as in **A**.

D. Early licking rate. Same mice as in **A**.

E. Latency of first lick during the response epoch for lick-left trials (left), lick-right trials (middle) and overlay of the two trial types (right). Bin size, 1 ms. Top, standard contingency; bottom, reversed contingency. There was no difference between the first lick latency between lick-left and lick-right trials (p>0.26, bootstrap, STAR Methods).

F. Distribution of recording depth of single units (from tasks 1-5). Recording depth is inferred from the manipulator. Most neurons are located between 400-900 um.

G. Single-unit classification in the left or right ALM. Putative fast-spiking interneurons and putative pyramidal neurons are separated based on the bimodal distribution of spike widths (STAR Methods). Inset, mean spike waveform of each unit.

H. Normalized selectivity (to each neuron's peak selectivity) of left-preferring neurons. White vertical bar, neurons with preparatory activity only. Gray bar, neurons with both preparatory activity and peri-movement activity. Black bar, neurons with peri-movement activity only.

I. Same format as in **H**, but for right-preferring neurons.

J. Fraction of selective neurons in different epochs. Selective neurons in each epoch were further split into left-preferring neurons (magenta) and right-preferring neurons (cyan).

K-N, Same format as G-J, but for the reversed contingency.

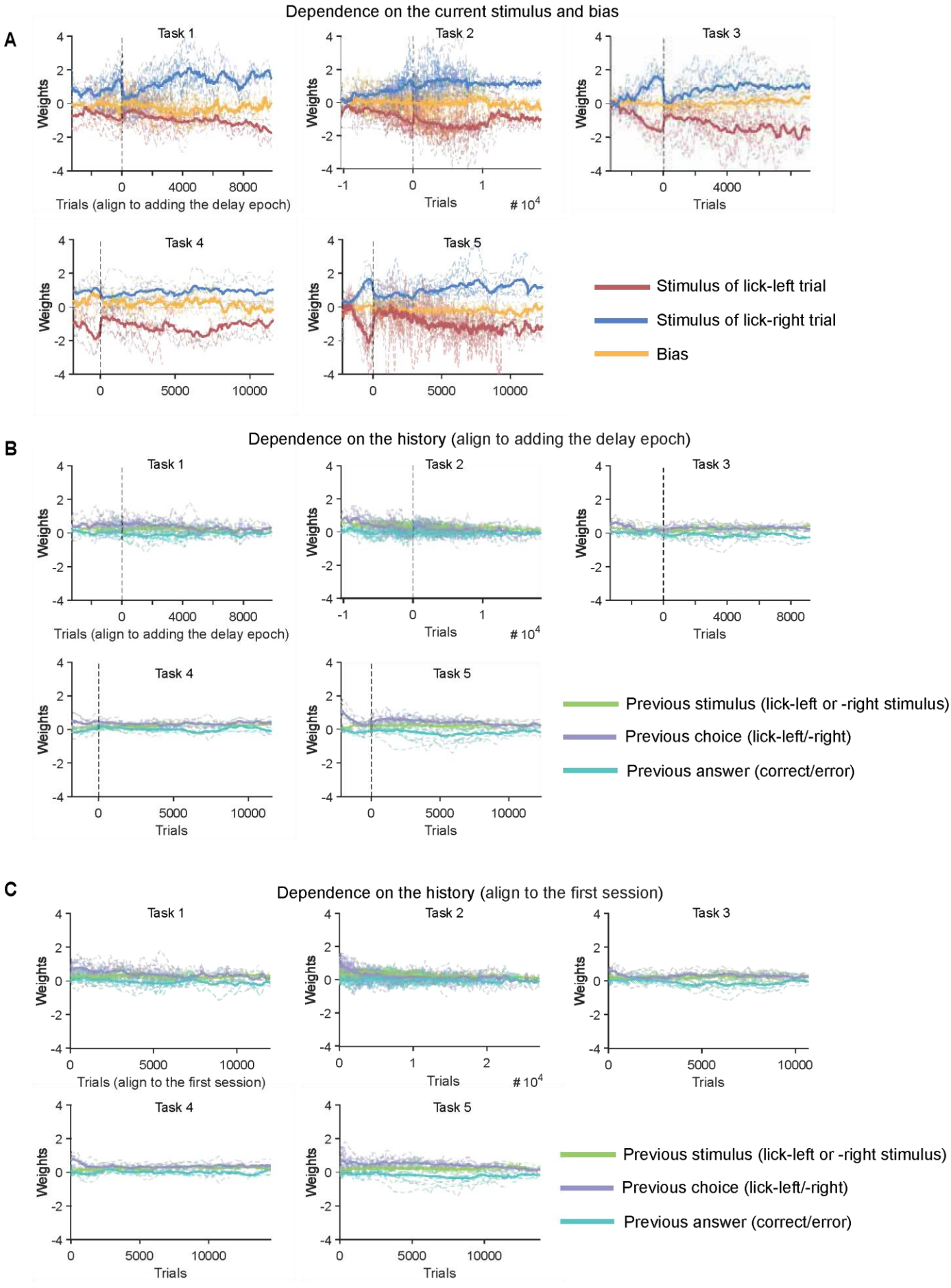
A
Dependence on the current stimulus and bias
Task 1
Task 2
Task 3
Task 4
Task 5
Weights
Trials (align to adding the delay epoch)
Trials
10^4
Stimulus of lick-left trial
Stimulus of lick-right trial
Bias
B
Dependence on the history (align to adding the delay epoch)
Previous stimulus (lick-left or -right stimulus)
Previous choice (lick-left/-right)
Previous answer (correct/error)
C
Dependence on the history (align to the first session)
Trials (align to the first session)

Figure S2. PsyTrack analysis to quantify behavioral bias and history dependence, Related to Figure 1.

A. Weights extracted using PsyTrack. Each dotted line denotes a mouse, and the solid line is the average (15, 22, 9, 7 and 14 mice for tasks 1-5, respectively). Trials are aligned to the introduction of the delay epoch. Mice gradually performed tasks based on whisker stimulation (red line, lick-left stimulus; blue line, lick-right stimulus). The bias (yellow line) was close to zero throughout training.

B. Similar to A, but for weights of history (the previous trial). Trials are aligned to the introduction of the delay epoch. Some mice exhibited dependence on the previous choice (purple line) during the early training, which was more obvious in **C**.

C. Same format as **B**, but trials are aligned to the first session.

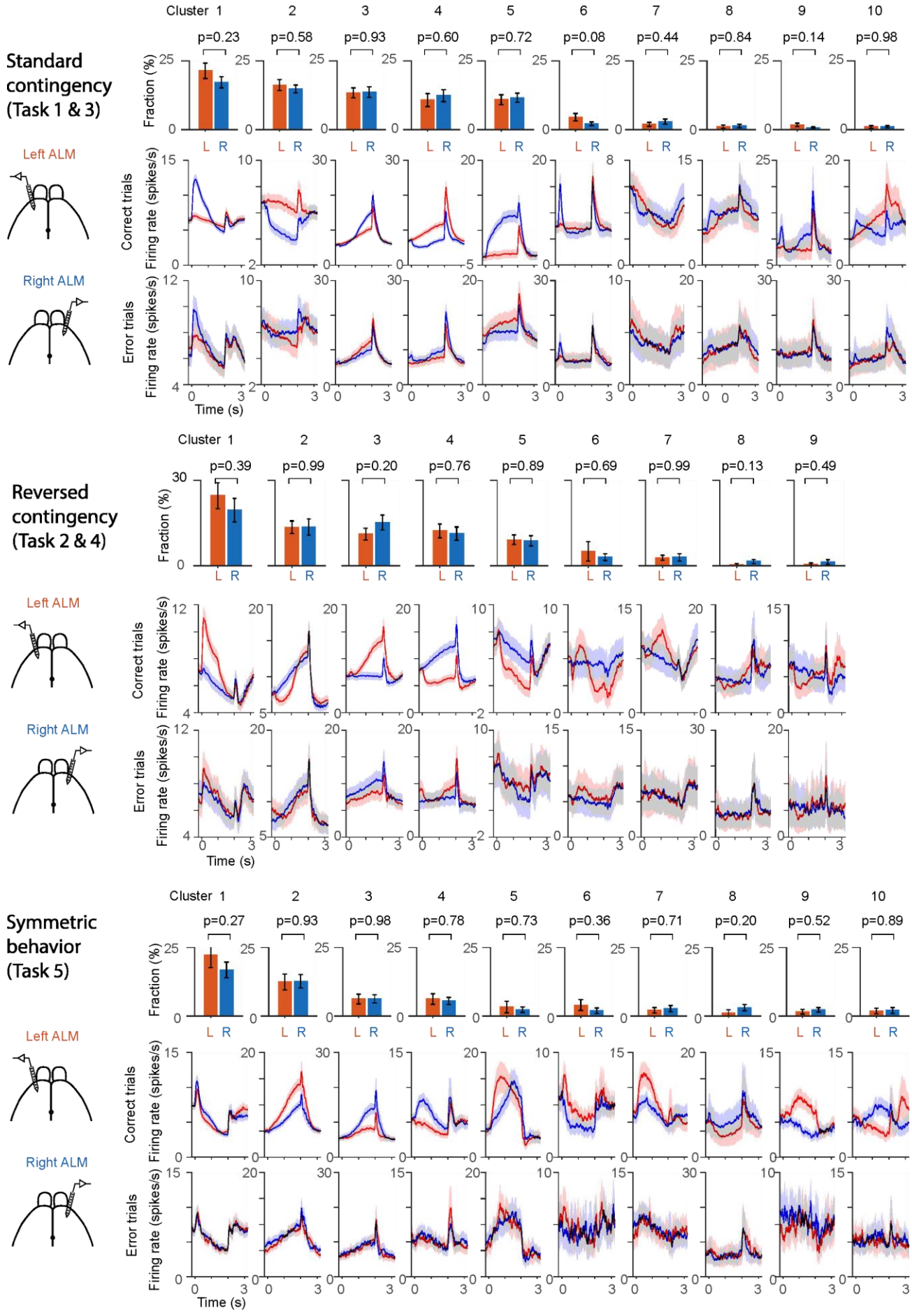
Standard contingency (Task 1 & 3)
Left ALM
Right ALM
Cluster 1 2 3 4 5 6 7 8 9 10
p=0.23 p=0.58 p=0.93 p=0.60 p=0.72 p=0.08 p=0.44 p=0.84 p=0.14 p=0.98
Fraction (%)
L R
Correct trials Firing rate (spikes/s)
Error trials Firing rate (spikes/s)
Time (s)
Reversed contingency (Task 2 & 4)
Left ALM
Right ALM
Cluster 1 2 3 4 5 6 7 8 9
p=0.39 p=0.99 p=0.20 p=0.76 p=0.89 p=0.69 p=0.99 p=0.13 p=0.49
Fraction (%)
L R
Correct trials Firing rate (spikes/s)
Error trials Firing rate (spikes/s)
Time (s)
Symmetric behavior (Task 5)
Left ALM
Right ALM
Cluster 1 2 3 4 5 6 7 8 9 10
p=0.27 p=0.93 p=0.98 p=0.78 p=0.73 p=0.36 p=0.71 p=0.20 p=0.52 p=0.89
Fraction (%)
L R
Correct trials Firing rate (spikes/s)
Error trials Firing rate (spikes/s)
Time (s)

Figure S3. Neuronal-response types in the left and right ALM are similar, Related to Figure 3.

A. Unsupervised hierarchical clustering of neurons recorded in tasks under the standard contingency (task 1 and 3). There are clusters preferring lick-right trials (for example, clusters 1, 3 and 5), preferring lick-left trials (clusters 2 and 4). Neurons in clusters 7 and 8 do not discriminate trial types and ramp up or down during the sample and delay epochs. In error trials, the preference was changed in some clusters (such as cluster 2-5), indicating that neurons in these clusters encode choice. Top, fraction of neurons for each cluster in left and right ALM. The fractions were similar for each cluster. *p*-value was determined by bootstrapping to account for variance across sessions and animals. Shading, SEM.

B. Same format as in **A**, but for neurons recorded under the reversed contingency (tasks 2 and 4). There are clusters preferring lick-left trials (clusters 1 and 3), lick-right trials (cluster 2, 4 and 5).

C. Same format as in **A**, but for neurons recorded in task 5.

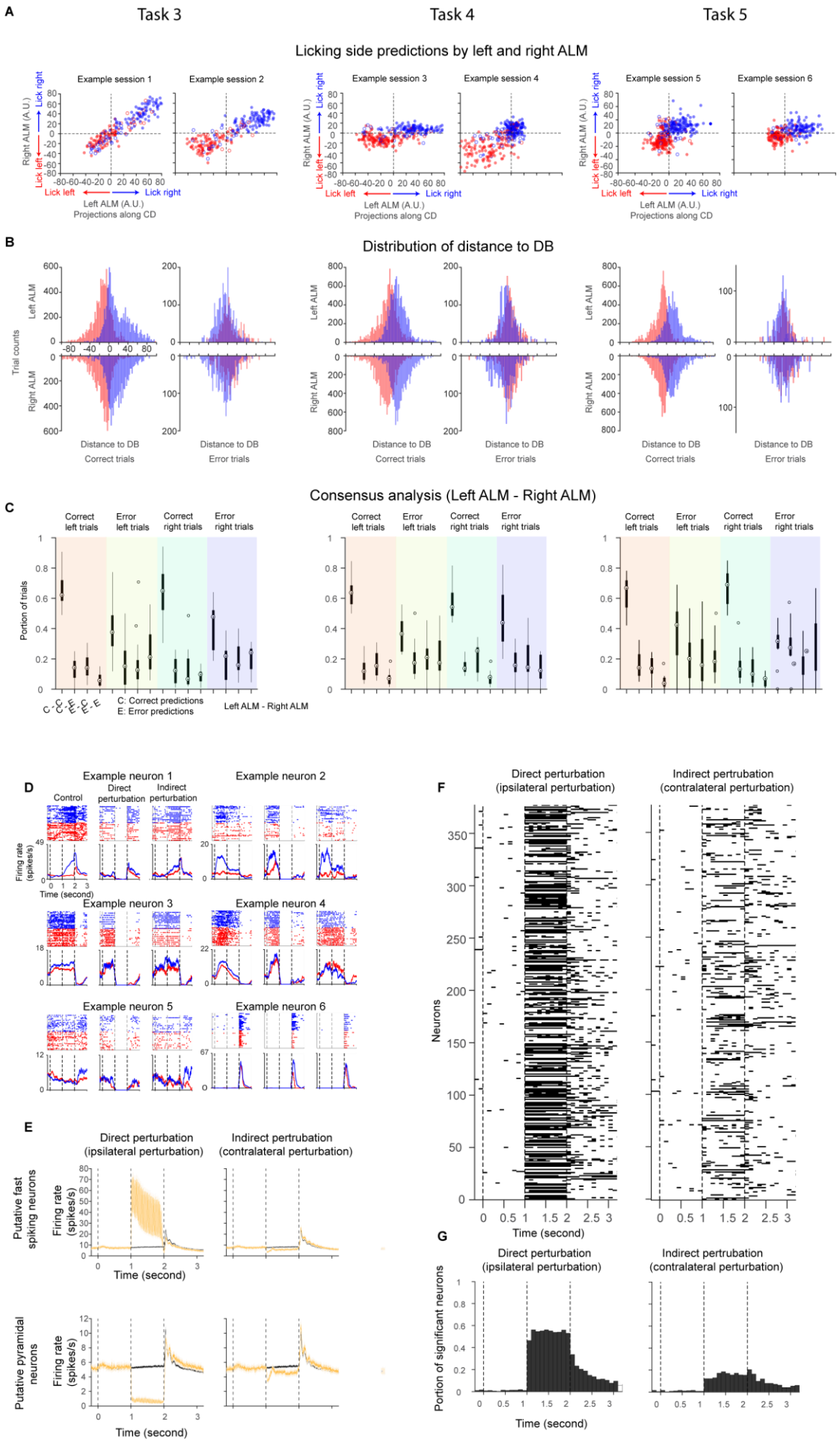
A
Task 3
Task 4
Task 5
Licking side predictions by left and right ALM
Example session 1
Example session 2
Example session 3
Example session 4
Example session 5
Example session 6
Right ALM (A.U.)
Lick right
Lick left
Left ALM (A.U.)
Projections along CD
B
Distribution of distance to DB
Trial counts
Left ALM
Right ALM
Distance to DB
Correct trials
Error trials
C
Consensus analysis (Left ALM - Right ALM)
Correct left trials
Error left trials
Correct right trials
Error right trials
Portion of trials
C: Correct predictions
E: Error predictions
Left ALM - Right ALM
D
Example neuron 1
Example neuron 2
Example neuron 3
Example neuron 4
Example neuron 5
Example neuron 6
Control
Direct perturbation
Indirect perturbation
Firing rate (spikes/s)
Time (second)
E
Direct perturbation (ipsilateral perturbation)
Indirect pertrubation (contralateral perturbation)
Putative fast spiking neurons
Putative pyramidal neurons
Firing rate (spikes/s)
Time (second)
F
Direct perturbation (ipsilateral perturbation)
Indirect pertrubation (contralateral perturbation)
Neurons
Time (second)
G
Direct perturbation (ipsilateral perturbation)
Indirect pertrubation (contralateral perturbation)
Portion of significant neurons
Time (second)

Figure S4. Single-trial decoding of choice with population activity sampled with simultaneous bilateral recordings, and electrophysiological characterization of unilateral inhibition, Related to Figure 4 and 5.

A. CD projection values at the end of delay epoch in example sessions for different tasks. A linear decoder is constructed by comparing trajectory endings with the decision boundary. Neural trajectory is projected along the coding direction (CD) that is determined for each hemisphere separately. The left and right ALM show consistent predictions on most of trials (dots in the upper right and bottom left quadrants). Blue circles, lick-right trials according to whisker stimulation strength. Red circles, lick-left trials. Filled circles, correct trials; open circles, error trials.

B. Distributions of CD projection values in correct and error trials. Red, lick-left trials. Blue, lick-right trials. In error trials, projection values in lick-left trials and lick-right trials largely overlap.

C. Portion of trials with same or conflict predictions based on CD projection values across hemispheres for different trial types (correct lick-left trials, error lick-left trials, correct lick-right trials and error lick-right trials). The fraction of same predictions in correct trials is higher across trial types and tasks.

D. Six example neurons recorded during direct and contralateral inhibition. Neurons are selected from the left or right ALM. Spike raster (top) and peri-stimulus time histogram (PSTH, bottom) are shown for each panel. Red, lick-left trials; blue, lick-right trials. Time is aligned to the sample start.

E. Mean PSTH of putative fast spiking (top) and putative pyramidal (bottom) neurons during direct (left panel) and contralateral (right panel) inhibition. Black, control. Orange, inhibition. Shading means SEM. Bin size, 1 ms. Smooth window, 2 ms.

F. Significant activity change indicated by black lines during direct (left panel) or contralateral inhibition (right panel). Each row represents a neuron. Significance is determined by comparing firing rates between control and perturbation trials ($p<0.01$, two sided *t*-test, bin size 100 ms).

G. Fraction of neurons significantly modulated by photoinhibition at different time bins.

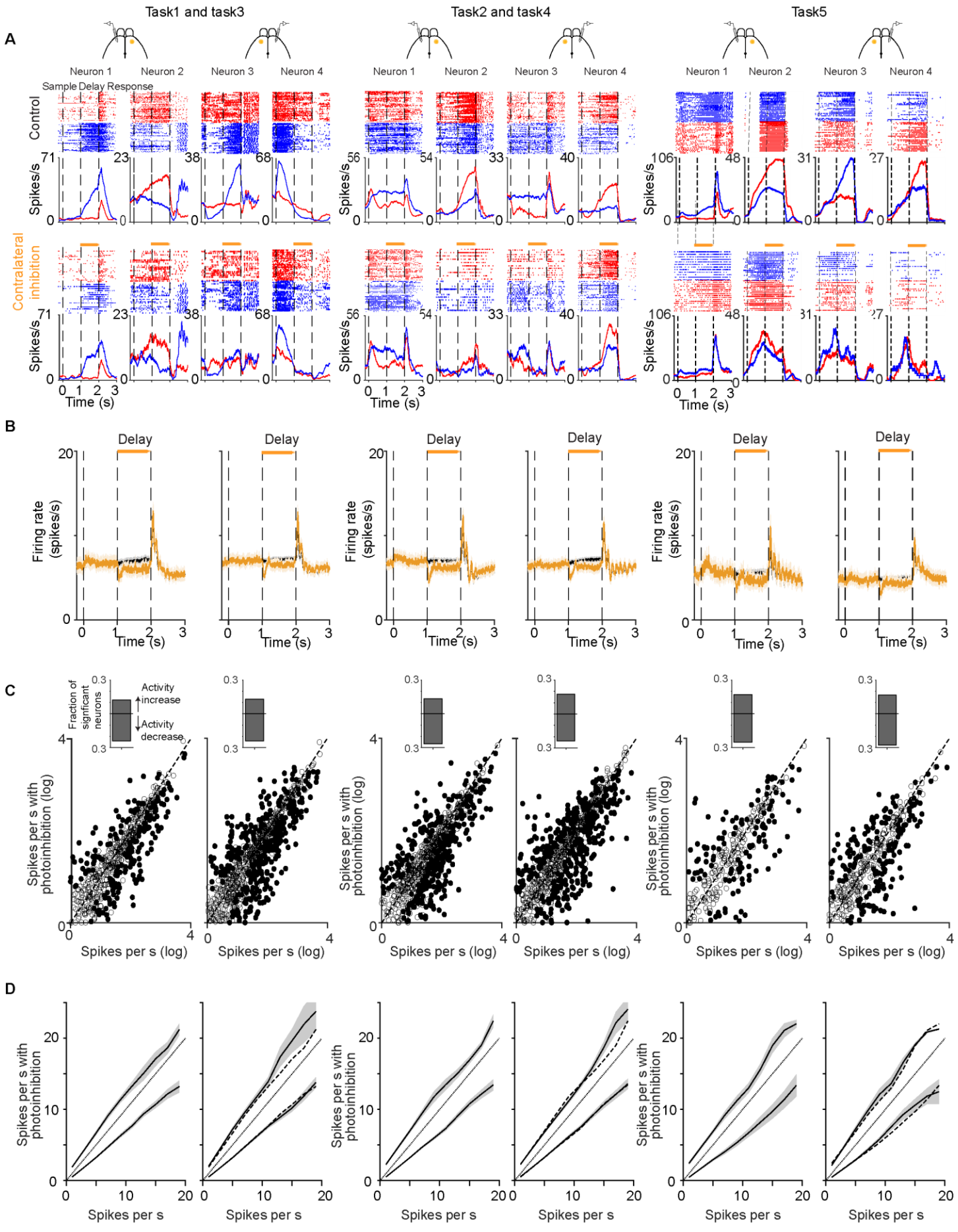
A
Task1 and task3
Task2 and task4
Task5
Neuron 1
Neuron 2
Neuron 3
Neuron 4
Sample Delay Response
Control
Contralateral inhibition
Spikes/s
Time (s)
B
Delay
Firing rate (spikes/s)
Time (s)
C
Fraction of signficant neurons
Activity increase
Activity decrease
Spikes per s with photoinhibition (log)
Spikes per s (log)
D
Spikes per s with photoinhibition
Spikes per s

Figure S5. Unilateral inhibition of the left or right ALM similarly affects contralateral neural activity at single neuron level, Related to Figure 6.

A. Example neurons in the left (neurons 1-2) and right (neurons 3-4) ALM. Top, control. Bottom, contralateral inhibition. Neuron in tasks under the standard contingency (tasks 1 and 3) or the reversed contingency (tasks 2 and 4) are pooled together as the behavioral deficit is similar.

B. Mean activity during control (black) and contralateral inhibition (orange) conditions. Shading, SEM.

C. Scatter plot of mean firing rates of individual neurons. There are similar fractions of neurons modulated across hemispheres in each task (Task 1 and 3, left ALM vs right ALM, 258/707 vs 416/1119, p=0.77; task 2 and 4, left ALM vs right ALM, 383/957 vs 479/1158, p=0.53; task 5, left ALM vs right ALM, 172/409 vs 253/567, p=0.42; *chi*-squared test). Filled circles, activity significantly changed by contralateral photoinhibition. Inset, fraction of significantly up-modulated and down-modulated neurons.

D. Relationship of firing rates in up-modulated and down-modulated neurons as a function of control activity. Dotted lines, relationship from the left panel shown for comparison. Shading denotes SEM.

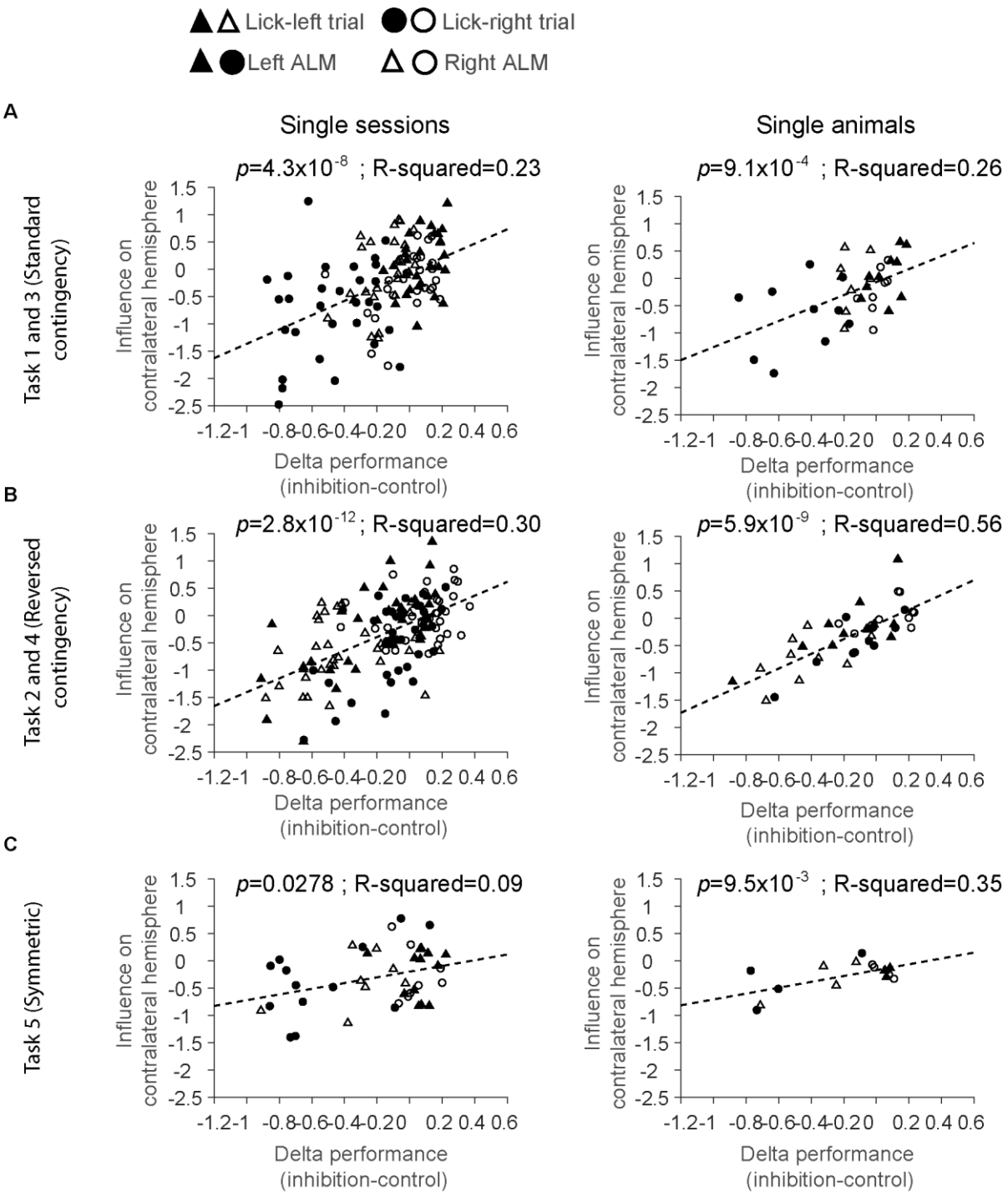

Figure S6. Behavioral deficit is linearly correlated with influence on the contralateral hemisphere in different tasks, Related to Figure 7.

A. Left panel, influence on the contralateral hemisphere is correlated with behavioral performance change for individual sessions. Influence on the contralateral hemisphere is quantified by the difference of the distribution along CD between control and inhibition trials (STAR Methods). Triangle, lick-left trial; circle, lick-right trial. Filled, left ALM inhibition; unfilled, right ALM inhibition. p-value and R-squared are shown on the top of each panel. Right panel, delta performance is correlated with the influence on the contralateral hemisphere for individual mice.

B. Same format as in **A**, but for the reversed contingency (task 2 and 4).

C. Same format as in **A**, but for task 5.

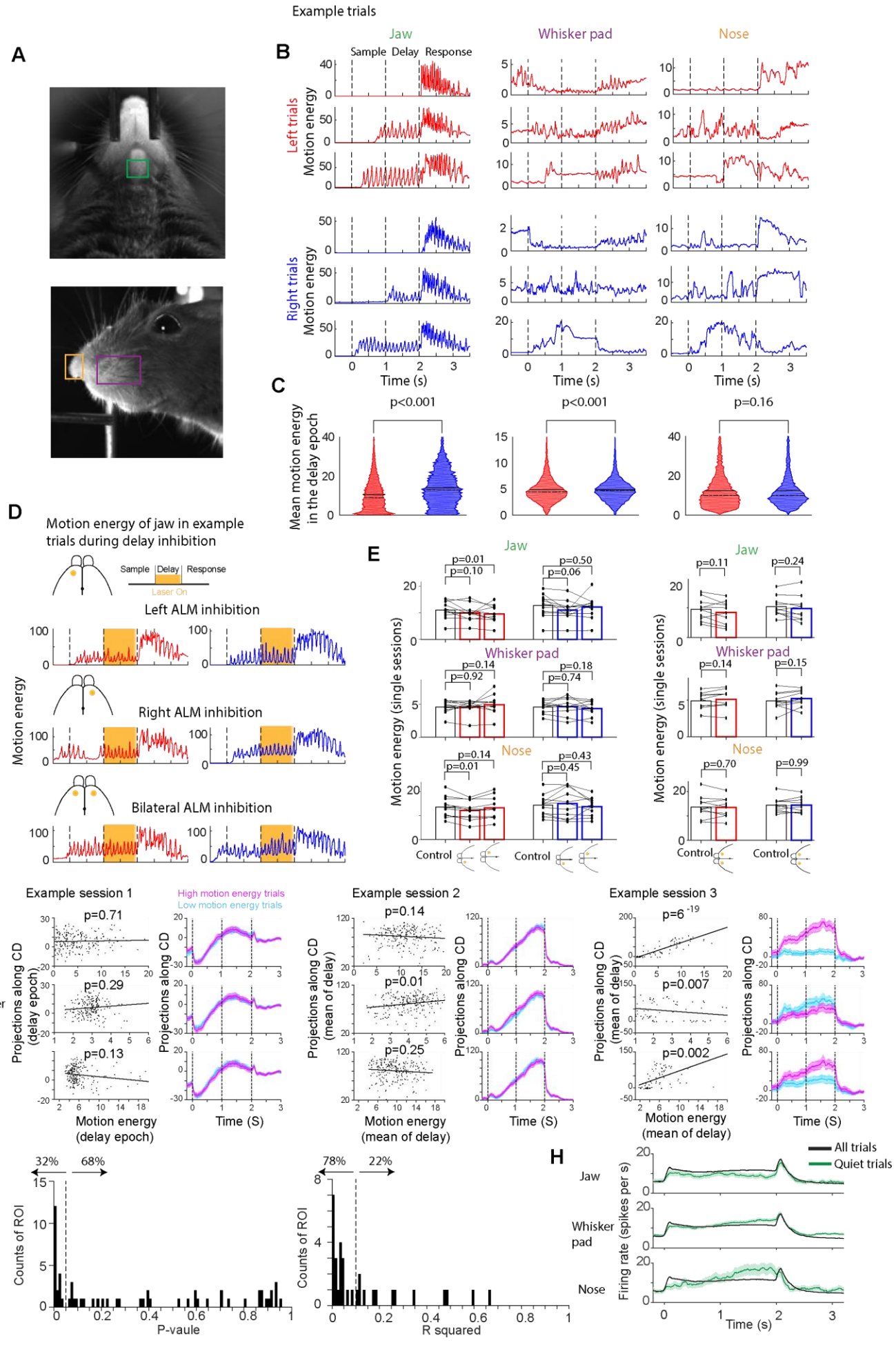
A
B
Example trials
Jaw
Whisker pad
Nose
Sample Delay Response
Left trials
Right trials
Motion energy
Time (s)
C
p<0.001
p<0.001
p=0.16
Mean motion energy in the delay epoch
D
Motion energy of jaw in example trials during delay inhibition
Sample Delay Response
Laser On
Left ALM inhibition
Right ALM inhibition
Bilateral ALM inhibition
Motion energy
E
Jaw
Whisker pad
Nose
Motion energy (single sessions)
p=0.01
p=0.10
p=0.50
p=0.06
p=0.11
p=0.24
p=0.14
p=0.92
p=0.18
p=0.74
p=0.14
p=0.15
p=0.14
p=0.01
p=0.43
p=0.45
p=0.70
p=0.99
Control
F
Example session 1
Example session 2
Example session 3
High motion energy trials
Low motion energy trials
Jaw
Whisker pad
Nose
p=0.71
p=0.29
p=0.13
p=0.14
p=0.01
p=0.25
p=6 -19
p=0.007
p=0.002
Projections along CD (delay epoch)
Projections along CD (mean of delay)
Motion energy (delay epoch)
Motion energy (mean of delay)
Time (S)
G
32%
68%
78%
22%
Counts of ROI
P-vaule
R squared
H
All trials
Quiet trials
Jaw
Whisker pad
Nose
Firing rate (spikes per s)
Time (s)

Figure S7. Relationship between orofacial movements and ALM neural activity, Related to Figure 7.

A. Example frames from videos recording orofacial movements from the bottom (top) and the side (down) cameras. Rectangles represent regions of interest (ROI) of the jaw, whisker pad and nose.

B. Example traces of motion energy (ME) from the three ROIs shown in **A**. Red, lick-left trials according to whisker stimulation strength. Blue, lick-right trials. All trials selected are correct trials. ME in different trials are variable.

C. Violin plot of mean ME during the delay epoch. Correct lick-left (red) and lick-right (blue) trials were selected. P-value is determined using Mann-Whitney U test. Data are from 55 sessions in 4 mice.

D. Example traces of ME for the jaw during inhibition of the left ALM (top), right ALM (middle) or bilateral ALM (down). Inhibition during the delay epoch is randomly deployed in 25% of trials.

E. Mean ME of individual sessions during inhibition of the left or right ALM inhibition (left panel), and bilateral ALM (right panel). Each line represents one session, and the bar denotes the mean value. P-value is determined by paired *t*-test.

F. The relationship between ME and CD-projected neural activity in three example sessions. Each dot denotes one trial. The solid line is the linear regression. The right panes for each session show CD-projected neural activity in low and high motion energy trials (trials are split in half based on the motion energy to get low motion energy and high motion energy trials). In example sessions 1 and 2, there are almost no correlations between CD-projected activity and ME as manifested by the large P-values. In example 3, the correlation is significant. For simplicity, CD-projected neural activity are shown for lick-right trials only (results are similar for lick-left trials).

G. Distribution of P-values (left panel) and fitted R-squared values (right panel). Data for ME of the jaw, whisker pad and nose are pooled together (30 ROIs from 10 sessions). Most P-values are greater than 0.05, indicating that CD-projections are poorly correlated with ME. R-squared values are small, implying that CD-projected neural activity is poorly explained by ME in most sessions.

H. Peri-stimulus time histogram (PSTH) of ALM activity in quiet (green) and all (black) trials. Quiet trials are selected based on jaw, whisker pad and nose movements separately (STAR Methods). Solid line is the mean. Shading denotes SEM. Shown is activity of the right-preferring neurons in lick-right trials where activity increase is robust. There is evident activity in quiet trials, and the magnitude during the delay epoch is significantly larger than that in the pre-sample epoch ($P<0.0001$ for all 3 ROIs; Mann-Whitney U test).